Received: 15 January 2019 | Revised: 19 June 2019 | Accepted: 18 September 2019

DOI: 10.1002/gj.3664

WILEY

RESEARCH ARTICLE

An ensialic volcanic arc along the northwestern edge of Palaeotethys—Insights from the Mid-Triassic volcano-sedimentary succession of Ivanščica Mt. (northwestern Croatia)

Damir Slovenec[1] | Branimir Šegvić[2] | Josip Halamić[1] | Špela Goričan[3] | Giovanni Zanoni[2]

[1] Department of Geology, Croatian Geological Survey, Zagreb, Croatia

[2] Department of Geosciences, Texas Tech University, Lubbock, Texas, USA

[3] Ivan Rakovec Institute of Palaeontology, ZRC SAZU, Ljubljana, Slovenia

Correspondence
Damir Slovenec, Croatian Geological Survey, Sachsova 2, Zagreb HR-10 000, Croatia.
Email: damir.slovenec@hgi-cgs.hr

Funding information
Croatian Ministry of Science, Education and Sport, Grant/Award Number: 181-1951126-1141; Javna Agencija za Raziskovalno Dejavnost RS, Grant/Award Number: P1-0008; National Science Foundation (USA), Grant/Award Number: MRI 04-511; Slovenian Research Agency, Grant/Award Number: P1-0008

Handling Editor: E. Bozkurt

This work aims to unveil the origin, geodynamic significance, and diagenetic history of pyroclastites and associated chert documented within the Upper Anisian volcano-sedimentary succession of the Ivanščica Mt. in Central Europe. An abundance of pyroclastic material points to polyphase volcanic activity and deep-water sedimentation along the rim of an oceanic realm. Radiolarian-based dating revealed Illyrian age of chert intercalated with pyroclastites. The latter are largely vitro-crystalloclastic and were emplaced as airborne tuff. The crystalloclasts of sanidine, plagioclase, altered pyroxene, and amphibole are principal tuff constituents merged in the altered glassy matrix consisted of palagonite, clay minerals, and calcite. Variations in alteration assemblages reflect an extensive in situ eogenesis in an open hydrologic system that gradually evolved toward a restricted fluid percolation environment. Mineralogy, chemistry, and occurrence of andesitic tuff clearly denote an explosive volcanic activity formed at the top of suprasubduction zone. Such scenario presumes a complex genesis outlined in following steps: (a) partial melting and dehydration of down-going Palaeotethyan slab which gave rise to the subduction-related magmatism {LILE, Th, and LREE [$(La/Lu)_{cn}$ = 6.51–9.42] enrichment; negative anomalies of Nb-Ta, P, and Ti [e.g., $(Nb/La)_n$ = 0.31–0.44]}; (b) magma contamination via interaction with continental crust during magma uplift along tectonically weakened zones of upper crust [positive Pb spikes, negative ε_{Nd} (−4.18 to −4.44), and $^{147}Sm/^{144}Nd \leq 0.113175$]. This is in favour of geodynamic evolution that hypothesizes the existence of an active, ensialic, and mature volcanic arc developed along the southern active continental margins of Euramerica (Laurussia) during Late Anisian subduction of Palaeotethyan lithosphere.

KEYWORDS

active continental margin, Croatia, ensialic volcanic arc, Ivanščica Mt., Middle Triassic volcano-sedimentary succession, Palaeotethys, palagonitization

1 | INTRODUCTION

The existence of the mid-Triassic Tethyan volcanism spatially and genetically linked to the onset of the formation of the Tethyan Mesozoic Adriatic–Dinaridic carbonate platform(s) and, then, its further disintegration is nowadays widely accepted (e.g., Castellarin, Lucchini, Rossi, Selli, & Simboli, 1988; Kovács, 1989; Philip, Masse, & Camoin, 1995; Vlahović, Tišljar, Velić, & Matičec, 2005; Robertson, 2007; McCann, 2008 and references therein; Storck, Brack, Jörn-Frederik Wotzlaw, & Ulmer, 2018). The mid-Triassic geodynamic evolution in

the areas of the Southern Alps, Dinarides, Hellenides, and Alpine-Carpathian Belt is, on the other hand, still largely debated. One school of thought relates the mid-Triassic developments to the continental rifting (e.g., Aljinović, Kolar-Jurkovšek, Jurkovšek, & Hrvatović, 2010; Borojević-Šoštarić, Neubauer, Handler, & Palinkaš, 2012; Crisci, Ferrara, Mazzuoli, & Rossi, 1984; Del Piaz & Martin, 1998; Harangi et al., 1996; Knežević, Jovanović, Memović, & Resimović, 1998; Kovács, 1992; Pamić, 1984; Pamić & Balen, 2005; Saccani, Dilek, Marroni, & Pandolfi, 2015; Velledits, 2004, 2006), while the other links them to convergent plate movements triggered by the subduction of Palaeotethys (e.g., Bébien et al., 1978; Bonadiman, Coltorti, & Siena, 1994; Casetta, Coltorti, & Marrocchino, 2018; Castellarin et al., 1980; Castellarin et al., 1988; Grimes, Wooden, Cheadle, & John, 2015; Kovács, 1992; Obenholzner, 1991; Schmid, Fügenschuh, Kissling, & Schuster, 2004; Smirčić, 2017; Smirčić et al., 2017; Stampfli & Borel, 2002, 2004; Storck et al., 2018; Trubelja, Burgath, & Marchig, 2004 and references therein). Both schools, however, agree on the existence of mid-Triassic oceanic basins of west Tethys (e.g., Chiari, Marcucci, Cortese, Ondrejičkova, & Kodra, 1996; Halamić & Goričan, 1995; Kozur, 1991; Tekin, Göncüoglu, & Turhan, 2002) formed as a result of Palaeotethyan back-arc magmatism (e.g., Robertson, 2002; Stampfli & Borel, 2002, 2004; Stampfli, Mosar, Pillevuit, & Vannay, 2001; Ziegler & Stampfli, 2001). These oceanic realms include the Küre, Meliata, and Maliak basins and most of the Triassic arc–back-arc system preserved in the Southern Alps, Alpine-Carpathian Belt, Dinarides, and Hellenides (e.g., Bortolotti et al., 2013; Castellarin et al., 1988; Chiari et al., 2012; De Bono et al., 2001; Dosztály & Jozsa, 1992; Goričan, Halamić, Grgasović, & Kolar-Jurkovšek, 2005; Ivan, 2002; Kiss, Molnár, Palinkaš, Kováacs, & Hrvatović, 2012; Ozsvárt & Kovács, 2012; Saccani et al., 2015; Slovenec, Lugović, Meyer, & Garapić-Šiftar, 2011; Slovenec, Lugović, & Vlahović, 2010; Stampfli & Borel, 2002). Taking into account a vivid magmatic activity that took place in the western part of Tethys (in its Alpine–Carpathian–Dinaric region), along the continental rims of the carbonate platform, the volcano-sedimentary records derived thereof represent a valuable source of information on the geodynamic evolution of the Triassic arc–back-arc system.

The current state of research of mid-Triassic pyroclastite of Ivanščica Mt. is limited to the rocks' petrographical characterization (e.g., Golub & Brajdić, 1970; Goričan et al., 2005; Marci, Šćavničar, & Sijarić, 1982; Marci, Ščavnićar, & Sijarić, 1984). Building on that knowledge, the purpose of this work is to provide a complex mineralogical, petrological, and geochemical investigation of tuffs and associated radiolarian cherts. Coupled with the dating of radiolarians, the present study aims to outline a geodynamic environment in which the analyzed pyroclastic rocks of Ivanščica Mt. most likely formed. This will surely complement our knowledge on the geodynamic evolution of the Tethyan northwestern oceanic branch.

2 | OUTLINE OF REGIONAL GEOLOGY AND DESCRIPTION OF THE STUDY AREA

The Ivanščica Mt., located in northern Croatia, is situated at the triple junction of three major geotectonic units—the southeastern Alps, the Dinarides, and the Tiszia continental block (Figure 1a). Along with other intra-Pannonian *Inselgebirge* like the Medvednica Mts., Kalnik, Strahinščica, Ravna Gora, and Desinić Gora, Ivanščica Mt. represents a SW segment of the Sava Unit (sensu Haas et al., 2000) or the Zagorje-Mid-Transdanubian shear Zone (ZMTDZ; sensu Pamić & Tomljenović, 1998; Figure 1b). The ZMTDZ is about 100 km wide and approximately 400 km long sheared belt sandwiched between the two regional fault systems: the Zagreb-Zemplin (ZZL) and the Periadriatic-Balaton lineament (PL-BL). The geological history of the ZMTDZ or Sava Unit is complex which is mirrored in its composition consisting of amalgamated Dinaric and South Alpine tectonostratigraphic fragments (e.g., Haas et al., 2000; Pamić & Tomljenović, 1998).

Mid-Triassic volcanic and volcanoclastic rocks from the north Croatian mountains (Figure 1b) are intercalated with mid-Triassic marine sediments (e.g., Goričan et al., 2005; Halamić, Slovenec, & Kolar-Jurkovšek, 1998; Marci et al., 1982, 1984; Šimunić, 1992; Šimunić & Šimunić, 1979; Slovenec et al., 2010; Slovenec et al., 2011). The volcanism is manifested by the submarine andesite to basalt lava flows accompanied by multiple explosive eruptions of volcanoclastic material. Basic petrographical characteristics and occurrences of mid-Triassic volcano-sedimentary succession from ZMTDZ may be correlated with the Triassic volcano-sedimentary series of the Meliata-Maliak arc–back-arc system (e.g., Goričan et al., 2005) and with those from the Dinarides (e.g., Pamić, 1984, 1997; Smirčić et al., 2017; Trubelja et al., 2004).

The Cerina geological section is located at northern slopes of the western part of Ivanščica Mt. (Figure 1c). Lower and middle portions of the section are composed of lithified tuffs, while its upper part is dominantly made of silica-rich shale, cherts, and radiolarian cherts (Figure 2). There is a general similarity between sampled pyroclastic rocks featured by varying contents of crystalloclasts and lithoclasts. Both are especially abundant in the lower portion of the section (samples ce-1 through ce-5). The transition between pyroclastite and chert is gradual, marked by an upward increase in silicification intensity (samples ce-19 through ce-23; Figure 2d). The silicification of tuffs may be explained by volcanic activity leading to seawater oversaturation with volcanogenic silica, which in turns creates an environment favourable for rock silicification and preservation of microfossils with shells made out of silica (e.g., Ščavničar, Ščavničar, & Šušnjara, 1984). Within the lower chert portion (26–29 m), tuffs are documented only in 2-cm thick layers (Figure 2/IV and 2/V) characterized by a sharp contact with neighbouring chert (Figure 2/V). The lower part of the section (samples ce-1 through ce-5; Figure 2) is marked by the massive, up to 2 mthick, coarse-grained varieties of grey–green tuff rich in crystalloclasts and rare lava lithoclasts that may attain up to 3 mm in diameter (Figure 2a). Due to an intensive fragmentation of the section's lower segment, some tuff samples have been brecciated (samples ce-2 and ce-4; Figure 2). Coarse-grained tuff varieties may also be found in the middle portion of the section (samples ce-14 through ce-17; Figure 2/III) being up to 30 cm thick and featured by a myriad of calcite veins. Pyroclastic material from the rest of the section emerges in the form of thin interlayers (up to 10 cm thick)

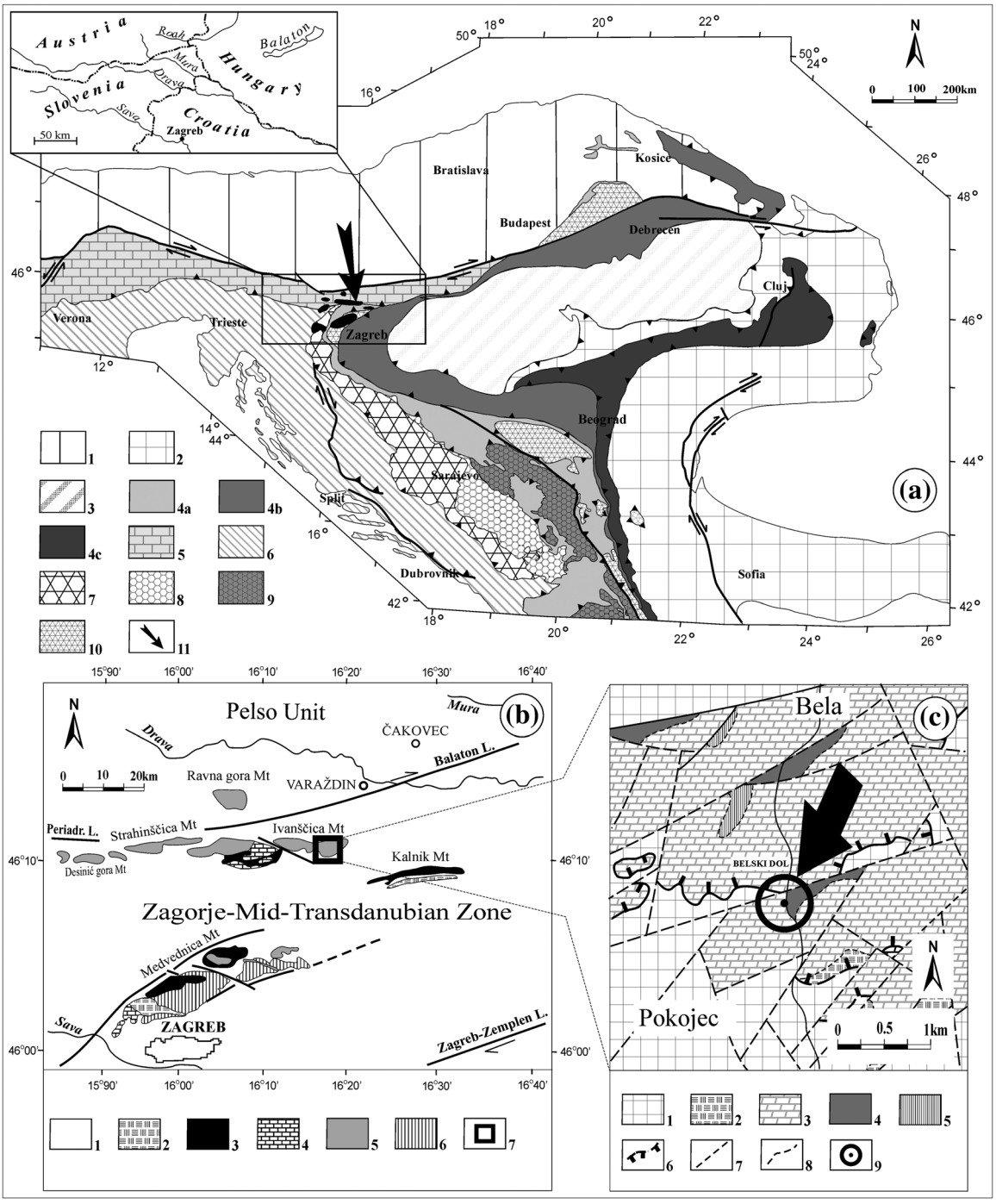

FIGURE 1 (a) Geotectonic sketch map of the major tectonic units of the Alps, Carpathians, and Dinarides (simplified after Schmid et al., 2008). The inset map (upper left corner): regional geographic overview. *Note*: 1 = Adria-derived far-travelled nappes Alps and W. Carpathians (ALCAPA); 2 = Europe-derived units (Dacia); 3 = mixed European and Adriatic affinities (Tisza); Ophiolites oceanic accretionary prisms: 4a = Meliata, Darnó-Sźarvaskö, Dinaric, Western Vardar, Mirdita; 4b = Piemont-Liguria, Vahicum, Inacovce-Kriscevo, Szolnok, Sava; 4c = Transylvanian, South Apuseni, Eastern Vardar; 5 = Southern Alps; 6 = Adriatic Plate, High Karst and Dalmatian Zone; 7 = Pre-Karst and Bosnian Flysch; 8 = East Bosnian-Durmitor; 9 = Drina-Ivanjica, Korab, Pelagonides; 10 = Bükk, Jadar, Kopaonik; 11 = black arrow indicates the Ivanščica Mt. investigated area. (b) Geological sketch map of the Croatian part of the Mid-Trandanubian Zone (slightly modified after Pamić & Tomljenović, 1998). *Note*: 1 = Quaternary and Neogene fill of the Pannonian Basin; 2 = Upper Cretaceous-Palaeocene flysch; 3 = Ophiolitic mélange (Kalnik Unit); 4 = Upper Triassic platform carbonates; 5 = Upper Palaeozoic and Triassic clastics and carbonates interlayered with volcanics and tuffs; 6 = Palaeozoic-Triassic metamorphic complex (Medvednica Unit); 7 = area more detailed shown on the geological sketch map C. (c) Simplified geological map of the southwestern part of Mt. Ivanščica (modified after Šimunić, Pikija, & Hećimović, 1982). *Note*: 1 = Neogene and Pleistocene sedimentary rocks; 2 = Jurassic-Cretaceous limestones; 3 = Middle Triassic limestones and dolomites; 4 = Middle Triassic shales, radiolarites, and tuffs; 5 = Lower Triassic clastics rocks; 6 = reverse or thrust faults; 7 = normal faults; 8 = discordance line, tectonic-erosion discordance; 9 = location of studied section

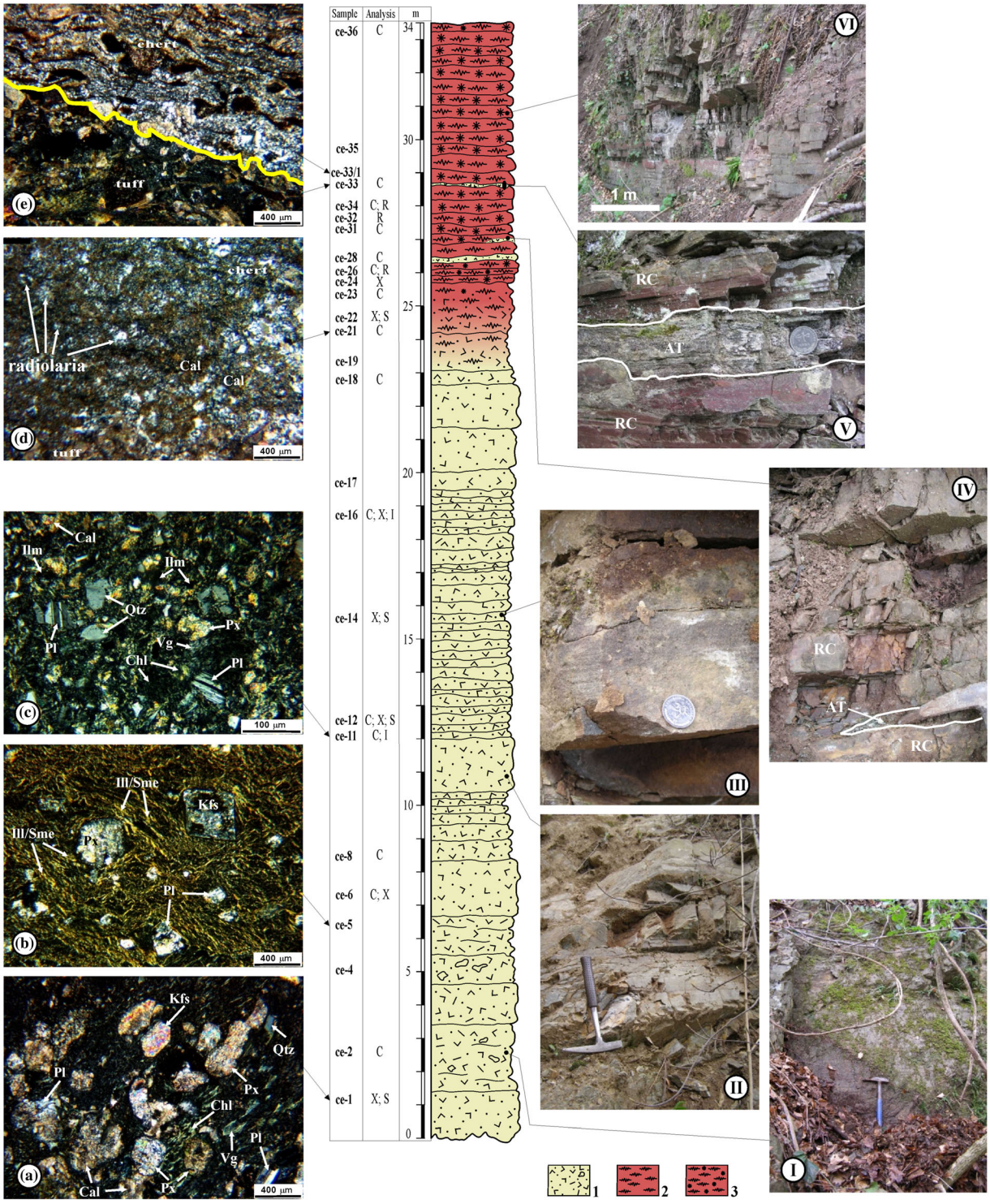

FIGURE 2 Lithological column "Cerina" of the investigated area (locality Belski Dol) in the southwestern part of the Mt. Ivanščica. *Note*: 1 = pyroclastic rocks (andesite tuffs; AT); 2 = cherts; 3 = radiolarian cherts (RC). Abbreviations for sample analysis: C = bulk-rock chemical analysis; X = XRD analysis; S = SEM-EDS analysis; I = isotope (Nd and Sr) analysis; R = analysis of radiolarians. Representative photographs of a (I) thick-layered coarse-grained vitro-crystallo-lithoclastic tuffs, (II) thick-layered fine-grained vitro-crystalloclastic tuffs, (III) thin-layered coarse-grained vitro-crystalloclastic tuffs, (IV and V) centimetre-thick interlayers fine-grained vitro-crystalloclastic tuffs in the radiolarian cherts, and (VI) thin- to medium-layered red cherts. Microphotographs of thin section of a (a) coarse-grained vitro-crystallo-lithoclastic andesite tuff (sample ce-1) N+, (b) vitro-crystalloclastic andesite tuff with abundance of illite–smectites (sample ce-5) N+, (c) fine-grained crystalloclastic andesite tuff (sample ce-11) N+, (d) gradual transition from fine-grained vitroclastic silicified andesite tuff to radiolarian chert (sample ce-21) N+, (e) sharp contact of coarse-grained vitro-crystalloclastic andesite tuff (sample ce-33) and Mn-enriched chert (sample ce-33/1) N+. Abbreviations: Cal, calcite; Chl, chlorite; Px, pyroxene; Ill/Sme, illite/smectite; Ilm, ilmenite; Kfs, K-feldspar; Pl, plagioclase; Qtz, quarz; Vg, volcanic glass [Colour figure can be viewed at wileyonlinelibrary.com]

composed of fine-grained tuff with rare crystalloclasts (Figure 2/II, 2/IV, and 2c). There is no report of normal and inverse grading in analyzed tuff, but a weak tendency of fining upward is preserved pointing to the grain size decrease in the tuff from deeper portions of the section, which defines a contact with radiolarian chert. Identified intercalations of pyroclastite with radiolarian chert from the upper part of the section (Figure 2) indicate a deposition of volcanic ash in a marine environment. Analyzed pyroclastic rocks are related to the sedimentation of airborne volcanic material, which is a result of multiphase volcanic eruptions. The sources of pyroclastic material are believed to have been at most a few hundred kilometres away from the area of their deposition (Cas & Wright, 1987; Fisher & Schmincke, 1984; Schminke, 2004).

The upper portion of the section is made of silica-rich red, reddish to grey-greenish rocks (Figure 2/V–VI) of laminated structure, which colour is chiefly controlled by ferruginous content. Rocks are identified as radiolarian chert, silicified radiolarian shale (Figures 2d and 3f), and silicified shale. Within the package of silica-rich rocks, rare intercalations of thin pyroclastite are documented (Figure 2).

3 | METHODS

Bulk-rock powders for chemical analyses of eight volcanoclastic and seven siliciclastic samples were analyzed by ICP-ES for major elements and ICP-MS for all trace elements at ACME Laboratories in Vancouver, Canada. International mafic rocks were used as standards. Major element and trace element concentrations were measured with accuracy better than 1% and 5%, respectively. Nd and Sr isotopic compositions of one bulk volcanoclastic rock sample was measured in CRPG in Vandoeuvre, France on Triton Plus mass spectrometer. Normalizing ratios of $^{86}Sr/^{88}Sr = 0.1194$ and $^{146}Nd/^{144}Nd = 0.7219$ were assumed. The $^{87}Sr/^{86}Sr$ ratio for the NBS 987 Sr standard for the period of measurement was 0.710242 ± 0.000030 (2σ). The $^{143}Nd/^{144}Nd$ ratio for the La Jolla standard was 0.5118451 ± 0.000010 (2σ). Total procedural blanks were ~500 and ~150 pg for Sr and Nd, respectively.

X-ray diffraction (XRD) was carried out on a set of seven representative samples (Table 1). For that purpose, the material was first gently crushed and powdered in an agate mortar and was thereupon placed in the sample holder for whole-rock measurements. Additionally, the diffraction on clay fraction (<2 μm) was performed on the same set of samples. Clay fraction was separated from the crushed material by centrifugation. Na metaphosphate was added to disperse the clays, followed by disaggregation using an ultrasonic bath. The clay fraction was further separated by centrifugation and saturated by Mg using a solution of 10 mL of ~4 M $MgCl_2$ to ensure a uniform cation exchange. Suspensions were washed and centrifuged with distilled water at least three times to minimize the content of free ions. The oriented mounts were prepared using a Millipore membrane filter. After the clay suspension was drawn onto the filter, it was left to dry at 50°C prior to the transfer to porous ceramic tiles. The measurement was taken in an air-dried condition and after saturation with ethylene glycol. Samples were scanned using a step mode in the Bragg–Brentano geometry (10 s/0.02°2Θ) over the range of 3 to 70°2Θ (global sample) and 3 to 30°2Θ (clay fraction; U = 30 kV, I = 15 mA; CuKα radiation) using a Rigaku Miniflex II installed at the Department of Geosciences, Texas Tech University, USA. Diffraction patterns were interpreted with the help of the Rigaku PDXL-Integrated X-ray powder diffraction software (V. 2.7.2.0, Tokyo, Japan) by comparing the experimental peaks with the published files provided by the International Centre for Diffraction Data (JCPDS 2000). XRD patterns of clay minerals were examined using the methods described by Moore and Reynolds (1997) and Środoń (2006).

To infer on the micromorphological characteristics and phase chemistry of pyroclastic material and its diagenetic alterations, SEM-EDS investigation by high-magnification back-scattered electron (BSE) and secondary electron (SE) imaging was performed using a Hitachi S-4300 E/N field emission variable pressure scanning electron microscope installed at the College of Arts and Sciences Microscopy of Texas Tech University, USA. Analyses were undertaken on a set of representative samples (Table 1) that were prepared as polished thin sections and then carbon coated. A variety of acceleration voltages and beam size conditions were employed to assure the best imaging conditions. The ancillary analytical system EDAX Pegasus 4040 was used for EDS spectra acquisition and quantification in a standardless mode. Chemical data were used as atomic percentages and were normalized to 100%.

Three samples have been examined for radiolarians. The samples were treated two to three times with diluted 5% hydrofluoric acid. Radiolarians were picked from residues under a stereomicroscope with magnification 50×. The final species identification was performed using a SEM Jeol JSM T-330A at the Ivan Rakovec Institute of Palaeontology, Research Centre of the Slovenian Academy of Sciences and Arts, Ljubljana.

4 | RESULTS AND INTERPRETATION

4.1 | Mineralogy and petrography

4.1.1 | Pyroclastic rocks

Polarization and electron microscopy investigation of the recovered pyroclastic material of the Cerina section classified it largely as the vitro-crystalloclastic tuff (Figure 3b–d). The vitroclastic and vitro-crystallo-lithoclastic varieties (Figures 3a and 4a) are found rarely and solely in the lower portion of the section (1–6 m; Figure 2). Rock fabric is vitrophyre (Figure 2d) to crystallo-vitrophyre (Figure 3b–d) with the latter exhibiting an occasional foliation in the middle portion of the section due to the preferential orientation of phyllosilicates (Figure 2b).

Throughout the section, a range of crystalloclasts and porphyroclasts is reported in the palagonitized and diagenetically altered glassy matrix. These inclusions may attain up to 2 mm in size accounting mostly for igneous plagioclase and K-feldspar as well as primary ferromagnesian minerals (Figure 2a–c). Euhedral *sanidine* is

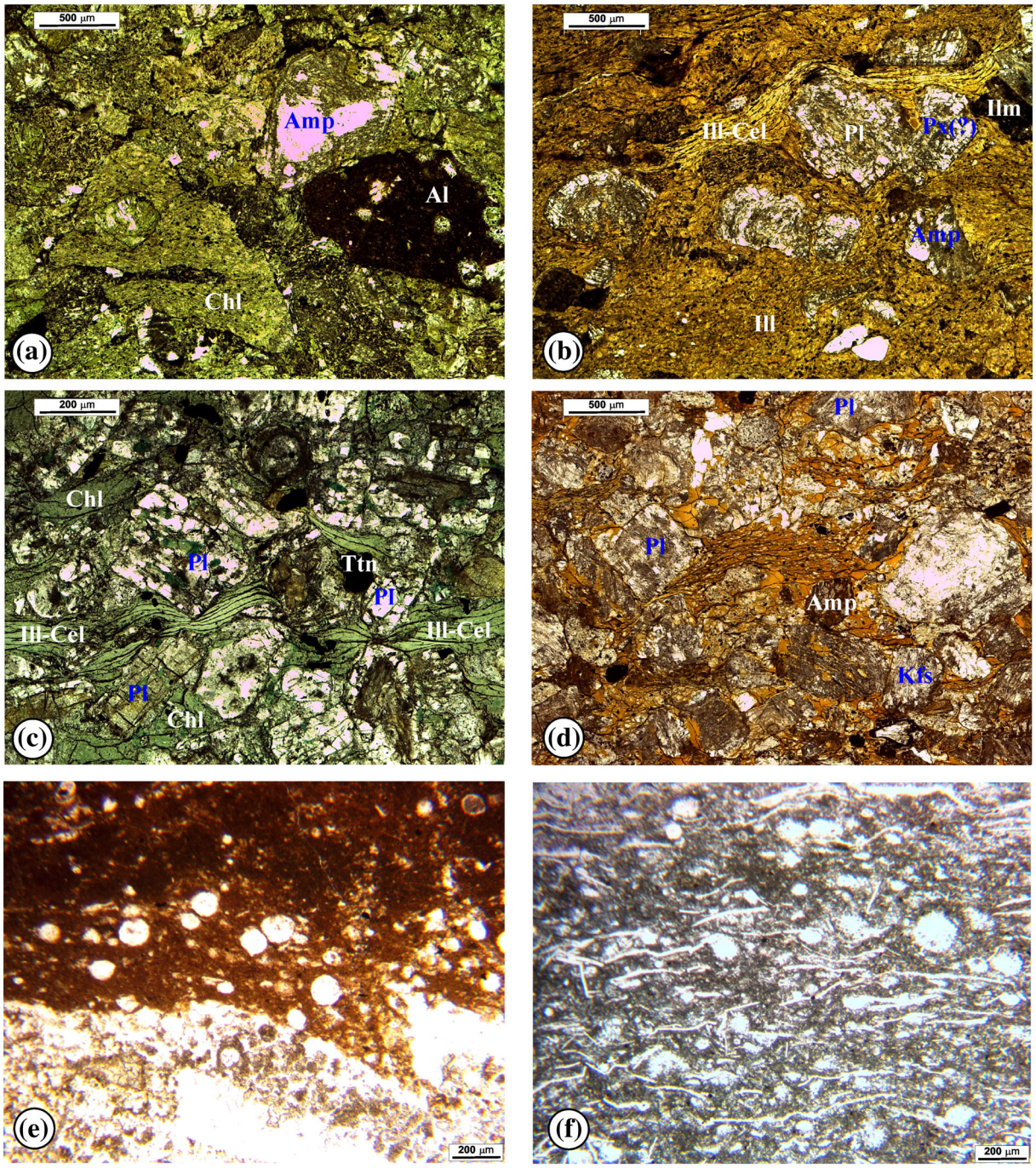

FIGURE 3 Microphotographs of thin sections of (a) coarse-grained vitro-crystallo-lithoclastic andesite tuff (sample ce-1) N−, (b) vitro-crystalloclastic andesite tuff (sample ce-6) N−, (c) fine-grained vitro-crystalloclastic andesite tuff (sample ce-12) N−, (d) vitro-crystalloclastic andesite tuff (sample ce-14) N−. (e) radiolarian chert (sample ce-21) N−, (f) siliceous shale to laminated chert with radiolarians and thin-shelled bivalves (sample ce-26) N−. Abbreviations: Amp, amphibole; Chl, chlorite; Px, pyroxene; Ill-Cel, illite-celadonite; Ilm, ilmenite; Kfs, K-feldspar; Pl, plagioclase; Ttn, titanite; Al, andesitic lava [Colour figure can be viewed at wileyonlinelibrary.com]

found in the base of the section being clearly corroded as well as partly replaced by secondary phases (Figure 4b; Table 2). *Plagioclase*, more than K-feldspar, is rather inhomogeneous (Figure 3b–d) and altered into a diverse paragenesis made of sericite, chlorite, and calcite, preserving only its relict outer shapes (Figure 2a,b). Rarely fresh, it is characterized by prismatic- and lath-shaped crystals with a typical polysynthetic twinning (Figure 2c). When in basaltic to andesitic lithoclastic inclusions, plagioclase is of bytownite to anorthite composition (Figure 4a; Table 2). Otherwise, its makeup corresponds to andesine to labradorite (Figure 4c,f; Table 2). Ferromagnesian component of analyzed tuffs has been entirely obliterated by secondary processes. It must have originally comprised *pyroxene* and/or *amphibole* (Figure 2a–c) then transformed into a mash of various Fe–Mg rich clay minerals and calcite (Figure 2a–c). In the middle portion of the section

TABLE 1 XRD analyses of the andesitic pyroclastic rocks from the Mt. Ivanščica

Sample	Whole rock	Clay fraction	Remarks
ce-1	Qtz, Cal, Kfs, Mi, Chl, Px(?)	Ab, Qtz, Chl, Mi (Fe), I-S, Ka(?)	Rich in chlorite; no discrete smectite; high illite–smectite
ce-6	Qtz, Kfs, Ab, Mi, Chl, Sme, Px(?), I-S	Qtz, Sme (Fe), Ab, Mi (Fe), Sme, I-S, Ka (?)	Two smectite species
ce-12	Qtz, An, Ab, Mi (Fe), Ca, Chl(?), Sme(?)	Sme (Fe), Sme, Mi (Fe), Ab, Ka(?), Chl(?), I-S(?)	Two smectite species; high mica content
ce-14	Qtz, Ab, Mi (Fe), Ca, Sme, Ka(?)	Sme (Fe), Sme, Mi (Mg), Qtz, Ka, Fs(?), I-S(?)	Two smectite species; high smectite content
ce-16	Qtz, Mi (Fe), Pl, Sme, Px(?)	Sme (Fe), Sme(?), Mi (Mg), Qtz, Ka, I-S(?)	High mica content
ce-22	Qtz, Ca, Mi (Fe), Pl, Sme, Ka	Sme, Mi (Mg), Mi, Ka	High mica content
ce-24	Mi (Fe), Mag, Qtz, Pl, Ka, Kfs	Qtz, Mi (Fe), Mi, Ka	No smectite

Abbreviations: Ab, albite; An, anorthite; Cal, calcite; Chl, chlorite; I-S, illite-smectite; Ka, kaolinite; Kfs, K-feldspar; Mag, magnetite; Mi, mica (Fe-Mg rich micaceous phase from the illite-alumoceladonite series); Qtz, quartz; Pl, plagioclase; Px, pyroxene; Sme, smectite.

(sample ce-14), relatively well-preserved mineral skeletons of presumably orthorhombic amphibole are documented (Figure 4g; Table 2). Although its phase chemistry does not reflect amphibole igneous origin, euhedral- to rod-shaped habit with a characteristic hexagonal base cut and cleavage angles leave no doubt that it used to be an amphibole. A detailed SEM investigation further revealed the presence of *muscovite* attaining up to 0.5 mm in size and showing some corrosion characteristics (Figure 4d,e; Table 2) like K-feldspar. The corrosion cavities are readily filled with illite, while at open fractures (Figure 4d; Table 2) and at mineral rims (Figure 4e; Table 2), main alteration phase is kaolinite. The observations on the nature of crystaloclasts recognized in analyzed rocks were corroborated by XRD measurements (Table 1) indicating quartz, feldspars, mica, and calcite as main phases. Quartz is usually not a crystalloclasts but rather a result of a complete or partial devitrification of volcanic glass (Figure 4c), while the presence of the terrigenous (e.g., allotriomorphic) quartz grains has not been documented. Further on, in the samples recovered from the top of the sections, radiolarians emerge as numerous silica inclusions (Figures 2d and 4h) in the palagonitized matrix. Based on XRD pattern comparison, it may be inferred that most of these opaline siliceous remains had transformed to quartz. Finally, at the lower portion of the Cerina section, the oval lithoclastic fragments of basaltic to andesitic lavas are reported (Figure 3a). They are up to 2 mm in size and featured by hypocrystalline texture defined by the laths of plagioclase enclosed in the glassy matrix, which is now largely palagonitized or converted to chlorite (Figure 4b; Table 2).

As shown by the microscopy and XRD investigation on clay fraction (Table 1), the fine-grained matrix that forms up to 90% of analyzed rocks is dominantly consisted of altered volcanic glass affected by different degrees of palagonitization and presumably, diagenesis at the later stage. Thus, the lower portion of the section is rich in illite–smectite, chlorite, and Fe-rich micas. Moving toward the main portion of the section (5–20 m; Figure 2), the matrix is consisted of two types of discrete smectite, a trioctahedral Fe-rich (saponite) variety, and Fe-poor species from the montmorillonite–beidelite series. Palagonitized, smectite-like matrix is usually intergrown with micron-sized quartz, hence, pointing to their genetic relationship (Figure 4f; Table 2). A few samples (e.g., ce-12) within the same array are characterized with two types of mica present in the fine fraction. First is fine-grained muscovite which is not an alteration product as previously mentioned, while the second stands for Fe-Mg rich member of the illite–alumoceladonite series (Figure 4e; Table 2). The latter is thought to present a final stage of evolution of the glassy component occasionally dominating the sample characterized with an intensive yellowish to greenish colour and parallel to subparallel cleavage (Figure 3b,c). Genetic relationship between the two micas is shown in Figure 4e, where the newly formed Fe-rich species encloses and absorbs the muscovite characterized by intrinsic instability. Lastly, at the section's upper portion that gradually changes into chert, volcanic glass seems to be homogenous and well preserved (Figure 4h). This variety also includes unaltered glass fragments with numerous, still visible, plagioclase laths. No discrete smectite was detected (Table 1); however, the chemistry of the glass reveals a complete transformation toward the cryptocrystalline paragenesis rich in mica from the illite–alumoceladonite series (Figure 4h; Table 2). Secondary calcite is present in the matrix throughout the section, while the opaque phases are sporadic and account for ilmenite and Fe-rich oxides (Figure 4c; Table 2).

4.1.2 | Sedimentary rocks

Silica-rich rocks of the upper portion of the section are mainly made of radiolarian cherts (samples ce-21, ce-31, ce-34/1, and 36; Figures 2d and 3e). The amount of radiolarian skeletons is relatively low and attains up to 15% of the rock. The spicules of sponges are determined in the sample ce-36. Rocks are reddish in colour due to the abundance of ferruginous substance, which is dispersed in the rocks, forming the submillimeter size agglomeration or parallel bands. The skeletons of radiolarians are up to 0.25 mm in diameter being largely recrystalized and filled with secondary calcite.

Second rock group is made of silicified shale featured by rare radiolarian skeletons and densely packed filaments (thin-shelled bivalves; samples ce-23 and ce-26; Figure 3f). Displaying a laminar structure, these rocks are marked by the alternation of centimetre-size laminae of pale red and grey silica-rich shale. The transition between laminae is gradual. Partly to completely recrystalized, calcified, and flattened radiolarian skeletons are occasionally found in the rock's matrix. Their size is between 0.15 and 0.25 mm. Accessory minerals are quartz and

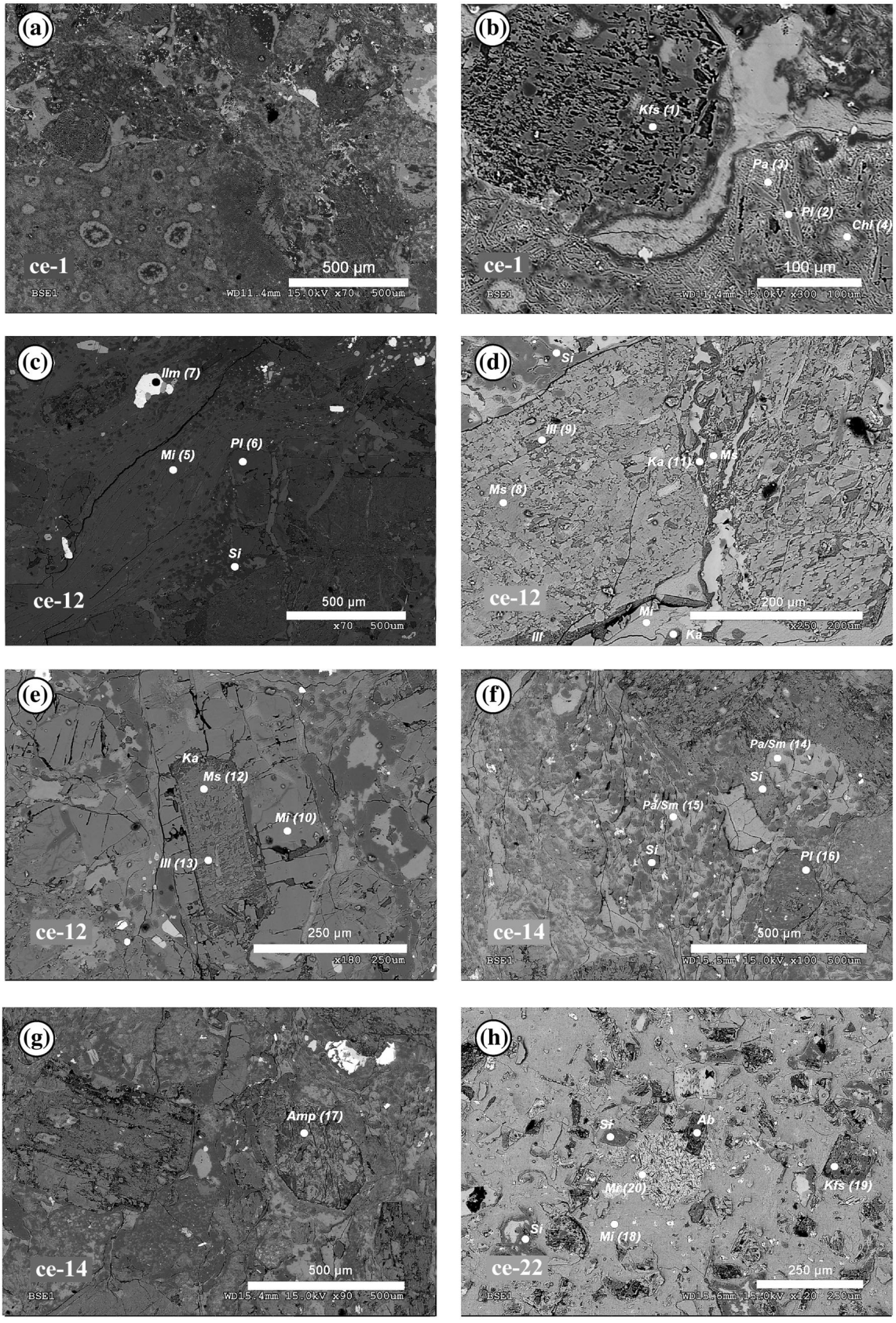

FIGURE 4 Back-scattered electron image of (a,b) coarse-grained vitro-crystallo-lithoclastic andesite tuff (sample ce-1), (c–e) fine-grained vitro-crystalloclastic andesite tuff (sample ce-12), (f,g) vitro-crystalloclastic andesite tuff (sample ce-14), and (h) vitrophyre andesite tuff (sample ce-22). Abbreviations: Amp, amphibole; Chl, chlorite; Ill, illite; Ilm, ilmenite; Kfs, K-feldspar; Pl, plagioclase; Ab, albite; Pa, palagonite; Pa/Sm, palagonite/smectite; Mi, mica; Si, silica; Ms, muscovite; Ka, kaolinite

TABLE 2 Selected EDS phase analyses (wt %) from the recovered pyroclastic material of Ivanščica Mt

Sample	ce-1	ce-1	ce-1	ce-1	ce-12	ce-12	ce-12	ce-12
Spectrum	1_Sp1	2_Sp2	3_Sp3	4_Sp4	5_Sp1	6_Sp2	7_Sp5	8_Sp6
Mineral	Kfs	Pa	Pl	Chl	Mi (?)	Pl	Ilm	Ms
SiO_2	52.96	47.40	54.41	42.81	59.51	56.99		50.19
Al_2O_3	34.90	18.27	29.55	15.07	15.52	26.86		36.62
FeO		21.43		27.60	10.14		49.60	1.56
MnO							2.52	
MgO	0.17	7.35		11.04	4.98			0.49
CaO			13.08			12.23		
Na_2O	1.31	1.60	2.96			3.92		0.30
K_2O	10.65	0.41		3.48	9.86			10.84
TiO_2		3.24					47.88	
Total	100.00	100.00	100.00	100.00	100.00	100.00	100.00	100.00

Sample	ce-12	ce-12	ce-12	ce-12	ce-12	ce-14	ce-14	ce-14
Spectrum	9_Sp7	10_Sp9	11_Sp11	12_Sp18	13_Sp19	14_Sp1	15_Sp5	16_Sp7
Mineral	Ill	Mi (?)	Ka	Ms	Ill	Pa/Sm	Pa/Sm	Pl
SiO_2	61.04	58.83	56.34	52.67	61.33	42.89	34.28	63.69
Al_2O_3	26.00	14.44	36.32	37.08	27.01	15.84	11.11	22.21
FeO	5.26	12.08	3.65	4.79	26.59	40.75		
MnO								
MgO	2.64	5.03	1.24	2.35	9.70	6.17		
CaO	3.93	1.68	3.97	2.13	2.60	9.94		
Na_2O						0.03		4.17
K_2O	1.13	9.62	0.77	10.25	0.55	2.50	5.09	
TiO2								
Total	100.00	100.00	100.00	100.00	100.00	100.00	100.00	100.00

Sample	ce-14	ce-22	ce-22	ce-22
Spectrum	17_Sp7	18_Sp1	19_Sp2	20_Sp5
Mineral	Amp (?)	Mi (?)	Kfs	Mi (?)
SiO_2	61.42	58.91	67.62	55.30
Al_2O_3	24.89	14.08	16.13	15.49
FeO	6.47	10.48	2.54	
MnO				
MgO	2.90	4.32		0.38
CaO	2.49	0.30	6.35	
Na_2O				0.40
K_2O	1.83	11.90	16.25	12.42
TiO_2			5.49	
Total	100.00	100.00	100.00	100.00

Note: Mi (?) stands for Fe-Mg rich micaceous phase from the illite–alumoceladonite series; Amp (?)—Altered primary inosilicate with chemistry significantly altered due to deuteric alterations. For details see the text.

Abbreviations: Amp, amphibole; Chl, chlorite; Ill, illite; Ilm, ilmenite; Ka, kaolinite; Kfs, K-feldspar; Mi, mica; Ms, muscovite; Pa, palagonite mixture; Pl, plagioclase; Sme, smectite.

mica. The former emerges in the form of semi rounded grains (up to 0.08 mm in size), while the latter renders tiny sheets that are up to 0.15 mm in size. Rocks are cut with submillimeter-size veins filled with hematite and to a lesser extent calcite.

Third rock group is consisted of completely silicified shale (sample ce-28), which is of grey–greenish colour and fine-grained texture cut with the veins of quartz. Iron agglomerations are commonly found in the form submillimeter-size lenses.

4.2 | Bulk rock chemistry

4.2.1 | Pyroclastic rocks

Chemical composition of the eight selected analyzed pyroclastic rocks is shown in Table 3. Their loss of ignition value (LOI) spans between 4.0 and 9.6 wt%. Since the latter may cause a mobilization of certain elements, we tested the element mobility by plotting elemental concentrations against the one of Zr (Figure 5), considering Zr content that figures as a standard differentiation index (e.g., Pearce, 1975; Shervais, 1982; Staudigel, Plank, White, & Schmincke, 1996). Significant mobilization of large-ion lithophile elements (LILE) such as Cs, Rb, K, and Ba is documented, while the high-field-strength elements (HFSE) like Th, Nb, Ta, Ti, P, Hf, Y, and rare-earth elements (REE) remained immobile during postmagmatic processes, and their concentration are thus mostly preserved. Transitional metals (V, Cr, Mn, Fe, Ni, and Sc) show moderate correlation with Zr and seem to have retained their magmatic abundance. Petrogenetic interpretations will therefore be based on HFSE and REE concentrations, while those of LILE and transitional metals are used with great caution. Analyzed pyroclastic rocks are classified as basalts and andesites of subalkaline characteristics (Figure 6a). Their elevated Ta/Yb ratios (0.22–0.28) and high Th/Yb ratios (3.3–4.8) are characteristic for the calc-alkaline to shoshonitic series (Figure 6b). A range of K concentrations in analyzed tuffs reflects either a variable modal abundance of K-feldspar, which is one of the basic products of volcanic activity (Lawrence, Drever, Anderson, & Brueckner, 1979), or higher proportion of micaceous phases. Alternatively, it can also partly results from late alteration processes and metasomatism, which usually leads to chemically distinct enrichment that is visually very subtle and therefore easily overlooked (Chapin & Lindley, 1985; Rajaraman, Nagendra Babu, Chavan, Achar, & Ramesh Babu, 2013). The enrichment in Na_2O documented in samples ce-11 and ce-18 (>2.54 wt %) reflects higher modal contents of plagioclase (Figure 2c). The Ivanščica Mt. tuffs are further characterized by low concentrations of V (82–176 ppm) as well as the other compatible elements like Cr (28–103 ppm) and Ni (5.4–20.0 ppm). Their relatively low values can be indicative of an evolved geochemical character of analyzed tuffs. Low values of Mg# (42.7–57.6) likely resulted from late mobilization of Fe and Mg (e.g., Jordan & Rippey, 2003; Figure 5). In the entire Cerina section, which comprises 23 m of deposited pyroclastic material, no regular distribution of elemental concentrations is documented (increase or decrease) going from the bottom toward the top of the section except for Fe_2O_{3total}, MgO, and Sc, which are impoverished in the tuffs from the top of the section (Figure 2; Table 3).

In the patterns of elemental abundance normalized to N-MORB, all rocks show significant LILE and Th enrichment with regard to HFSE (P, Zr, Hf, Ti, and Y) and mid- and heavy-rare-earth elements (MREE and HREE) ranging from 40 to 714 times and 0.7 to 4.8 times relative to N-MORB for the LILE/Th and HFSE group, respectively (Figure 7a). All rocks show the pronounced negative anomalies of the Nb–Ta pair relative to La [$(Nb/La)_{N\text{-}MORBn}$ = 0.31–0.44] as well as of P and Ti, which is typical for SSZ-related magmas. The Cerina tuffs are characterized by the positive Pb spikes relative to Ce [$(Pb/Ce)_{N\text{-}MORBn}$ = 2.68–11.24], while their normalized REE patterns show uniform trends and significant enrichment in LREE [$(La/Lu)_{Cn}$ = 6.51–9.42]. The MREE concentrations are only moderately enriched [$(Sm/Lu)_{Cn}$ = 2.41–2.79] whereas the fractionation patterns of HREE are subparallel and nearly flat [$(Tb/Lu)_{Cn}$ = 1.39–1.55] at 35.0–96.5 times and 8.4–17.1 times relative to chondrite for the LREE and HREE group, respectively (Figure 7b). All samples depict a negative Eu anomaly of high intensity (Eu/Eu^* = 0.62–0.76) typical for fractionation and removal of plagioclase (e.g., Sun & Nesbitt, 1978).

The values of the $^{143}Nd/^{144}Nd$ and $^{87}Sr/^{86}Sr$ ratios of two representative tuff samples show very narrow spans ranging from 0.512282 to 0.512299 and 0.707523 and 0.707562, respectively (Table 4). The initial ε_{Nd} and initial isotopic ratios of Sr were calculated for 245 Ma (Mundil, Pálfy, Renne, & Brack, 2010), which is the crystallization age of analyzed andesite tuffs based on the radiolarian dating in associated chert (see below). The initial ε_{Nd} varies between −4.18 and −4.44 while the initial $^{87}Sr/^{86}Sr$ ratio varies from 0.703745 to 0.706217. Very low values of the initial ε_{Nd} are characteristic for the subduction of continent-derived material (SCM; Swinden, Jenner, Fryer, Hertogen, & Roddick, 1990; Figure 8). The wide range of the $^{87}Sr/^{86}Sr$ ratio of analyzed samples that are particularly elevated in sample ce-11 likely calls for at the ocean-floor hydrothermal metamorphism (e.g., Bach, Peucker-Ehrenbrink, Hart, & Blusztajn, 2003; Coogan, 2009). These values are therefore excluded from further petrogenetic considerations.

4.2.2 | Sedimentary rocks

Chert chemistry is provided in Table 3 along with the ratios of several key elements and element groups calculated on the volatile-free basis. The content of Si in analyzed rocks varies from 37.82 to 88.32 wt %, increasing toward the top of the section. The Si/Si + Al + Fe values reported in cherts from the neighbouring Medvednica and Kalnik Mts. (Figure 2b) vary between 0.901 and 0.950 (Halamić, 1998; Halamić, Marchig, & Goričan, 2001), pointing to the biogenic origin of Si in these sediments (Rangin, Steinberg, & Bonnot-Courtois, 1981). Calculated Si/Si + Al + Fe values in this study are spanning from 0.702 to 0.929 (Table 3). More specifically, the values for samples ce-21, ce-26, ce-31, and ce-36 fall in the 0.920–0.929 span, while the values for samples ce-23, ce-28, and ce-34/1 vary between 0.702 and 0.771. First group of data is analogue to the ones reported by Halamić et al. (1998), suggesting a biogenic origin of Si. This is further indicated by the increased content of radiolarian skeletons in the rocks. The Si/Si + Al + Fe values reported for the first group somewhat exceeded the amounts documented in the Mediterranean cherts (0.8–0.9; Ruitz-Ortiz, Bustillo, & Molina, 1989) which could indicate a partial enrichment by the silica that originated from the chert/shale couplets. High negative correlation coefficients between Si and most of other elements point to dilution processes (e.g., Vine, 1969; Sugitani, Yamamoto, Wada, Binu-Lal, & Yoneshige, 2002; Table 3a). Samples from the second group are characterized by lower Si/Si + Al + Fe values, which is explained by the significant terrigenous impact and

TABLE 3 Chemical compositions of the andesitic pyroclastic rocks and cherts from Ivanščica Mt

Andesite tuffs								Cherts							
Sample	ce-2	ce-6	ce-8	ce-11	ce-12	ce-16	ce-18	ce-33	ce-21	ce-23	ce-26	ce-28	ce-31	ce-34/1	ce-36
Major oxides (wt %)															
SiO_2	53.10	57.40	56.50	58.04	54.06	56.64	56.48	56.56	76.64	46.97	69.81	63.41	90.48	77.93	83.80
TiO_2	0.86	1.03	0.81	0.54	1.00	0.65	0.70	0.68	0.11	0.76	0.12	0.39	0.09	0.10	0.15
Al_2O_3	15.97	15.39	17.18	16.31	19.29	15.85	15.91	15.88	3.05	11.95	2.96	11.93	2.05	2.09	3.28
Fe_2O_3total	6.69	6.77	6.90	4.52	5.37	3.80	4.65	3.62	1.68	4.27	1.58	4.65	3.73	13.89	1.77
MnO	0.12	0.05	0.14	0.07	0.09	0.05	0.10	0.07	0.44	1.14	0.74	0.43	0.11	0.41	0.65
MgO	3.38	3.20	3.45	1.67	2.23	2.29	1.71	1.70	0.78	2.02	0.62	1.87	0.50	0.59	0.51
CaO	5.33	1.78	5.56	6.84	5.34	3.93	5.03	4.48	15.52	26.21	22.97	13.58	1.92	3.77	8.48
Na_2O	2.22	1.08	1.90	2.54	1.87	1.66	3.01	3.34	0.11	0.54	0.10	0.17	0.09	0.21	0.30
K_2O	3.00	6.00	3.34	3.31	4.20	5.11	4.06	4.59	1.32	5.42	1.06	3.49	0.98	0.92	0.93
P_2O_5	0.19	0.24	0.20	0.18	0.17	0.22	0.18	0.19	0.34	0.82	0.07	0.07	0.04	0.08	0.14
LOI	9.04	6.90	4.00	5.80	6.27	9.60	8.10	8.80	-	-	-	-	-	-	-
Total	99.84	99.84	99.98	99.85	99.85	99.79	99.92	99.93	99.99	100.01	99.99	99.99	99.99	99.99	99.99
Trace elements (ppm)															
Cs	1.9	2.6	1.1	2.8	5.0	3.8	1.8	2.8	1.5	3.7	2.4	7.4	1.9	1.6	1.8
Rb	31.6	89.9	33.1	50.9	129.5	123	41.5	82.3	31.1	106.0	26.0	93.3	31.6	29.4	30.7
Ba	389	403	300	440	230	768	822	545	147	513	82	255	64	80	132
Th	8.7	11.1	12.3	12.4	7.1	10.8	13.8	12.3	2.1	5.6	2.4	11.8	1.6	1.7	2.6
Ta	0.6	0.7	0.7	0.6	0.5	0.6	0.7	0.7	0.1	0.4	0.2	0.8	0.1	0.1	0.1
Nb	8.8	11.8	12	10.6	8.5	10.3	12.3	11.3	1.5	7.0	2.2	7.0	1.8	1.8	2.7
Sr	276	281	351	366	269	315	365	340	50	85	78	71	24	55	43
Zr	127	158	187	149	114	148	164	156	27	128	36	187	29	34	38
Hf	3.9	4.4	5.5	4.9	3.4	4.4	5.4	4.9	0.7	3.4	1.0	5.4	0.7	0.7	1.0
Y	20.6	29.0	28.9	25.6	23.3	28.8	29.1	28.9	27.1	38.6	17.4	19.1	8.0	20.7	27.4
Sc	23	22	21	13	21	16	16	14	4	13	4	11	3	3	4
V	176	139	124	82	135	149	95	122	39	100	19	52	21	63	26
Cr	103	48	41	28	41	82	55	69	7	8	7	21	14	15	14
Ni	20	12	8	5	10	9	10	10	[a]10	22	[a]10	75	27	62	[a]10
Pb	9.9	10.9	33	12.2	4.9	22	11.9	12.1	12.4	26.0	55.2	104.4	39.2	127.0	16.5
Co	17.0	12.5	13.4	3.0	7.5	10.0	30.0	17.0	1.2	22.7	4.3	13.9	3.9	8.2	2.3
Zn	59	81	93	39	53	64	51	55	12	52	20	113	18	37	23
Rare-earth elements (ppm)															
La	25.00	30.70	33.40	32.70	20.70	35.40	32.00	33.70	27.40	37.60	19.80	21.40	10.30	11.00	20.80
Ce	54.30	64.90	73.40	67.50	45.60	75.40	73.20	74.30	52.00	67.40	24.00	29.60	13.60	10.20	23.30
Pr	6.39	7.92	8.72	7.86	5.93	8.79	8.45	8.62	6.66	8.26	4.68	5.03	2.36	2.79	4.79
Nd	27.50	33.00	35.20	31.40	24.90	35.20	32.70	33.95	26.50	32.20	18.80	20.20	9.40	12.40	20.20
Sm	5.11	6.44	7.03	6.00	5.32	6.59	6.56	6.58	4.81	6.47	3.78	3.51	1.75	2.61	4.30
Eu	1.13	1.35	1.50	1.44	1.24	1.46	1.24	1.35	0.85	1.50	0.72	0.62	0.34	0.62	0.87
Gd	4.82	6.06	6.47	5.58	5.07	5.85	5.66	5.76	4.54	6.46	3.19	3.40	1.49	2.86	4.51
Tb	0.72	0.94	0.99	0.89	0.78	0.91	0.93	0.92	0.72	1.02	0.55	0.53	0.28	0.52	0.83
Dy	3.73	5.36	5.53	4.87	4.23	4.95	5.00	4.98	3.97	5.85	3.23	3.07	1.65	3.58	4.87
Ho	0.80	1.08	1.08	0.97	0.84	1.00	1.02	1.01	0.74	1.11	0.58	0.59	0.30	0.77	0.94
Er	2.20	2.94	2.96	2.61	2.27	2.70	2.95	2.83	2.20	3.53	1.54	1.67	0.83	2.57	2.52

(Continues)

TABLE 3 (Continued)

Andesite tuffs								Cherts							
Sample	**ce-2**	**ce-6**	**ce-8**	**ce-11**	**ce-12**	**ce-16**	**ce-18**	**ce-33**	**ce-21**	**ce-23**	**ce-26**	**ce-28**	**ce-31**	**ce-34/1**	**ce-36**
Tm	0.31	0.45	0.44	0.41	0.32	0.39	0.4	0.42	0.31	0.54	0.23	0.28	0.12	0.42	0.35
Yb	2.12	2.89	2.80	2.72	2.17	2.63	2.86	2.75	1.94	3.69	1.18	1.80	0.80	2.57	2.13
Lu	0.32	0.43	0.43	0.41	0.33	0.39	0.44	0.42	0.31	0.56	0.20	0.20	0.14	0.36	0.33
Mg#	50.10	48.73	50.61	42.66	49.84	57.63	43.24	50.24	-	-	-	-	-	-	-
Si/Si + Al + Fe	-	-	-	-	-	-	-	-	0.93	0.70	0.93	0.76	0.92	0.77	0.93
Al/Al + Fe + Mn	-	-	-	-	-	-	-	-	0.52	0.62	0.48	0.64	0.29	0.10	0.50

Note: LOI = loss on ignition at 1,100°C. Mg# = 100 × molar [MgO/(MgO + FeOtotal)]. Values for the major elements are recalculated on volatile-free basis for cherts.

[a]The presented values are the half value of the detection limit of the analytical method.

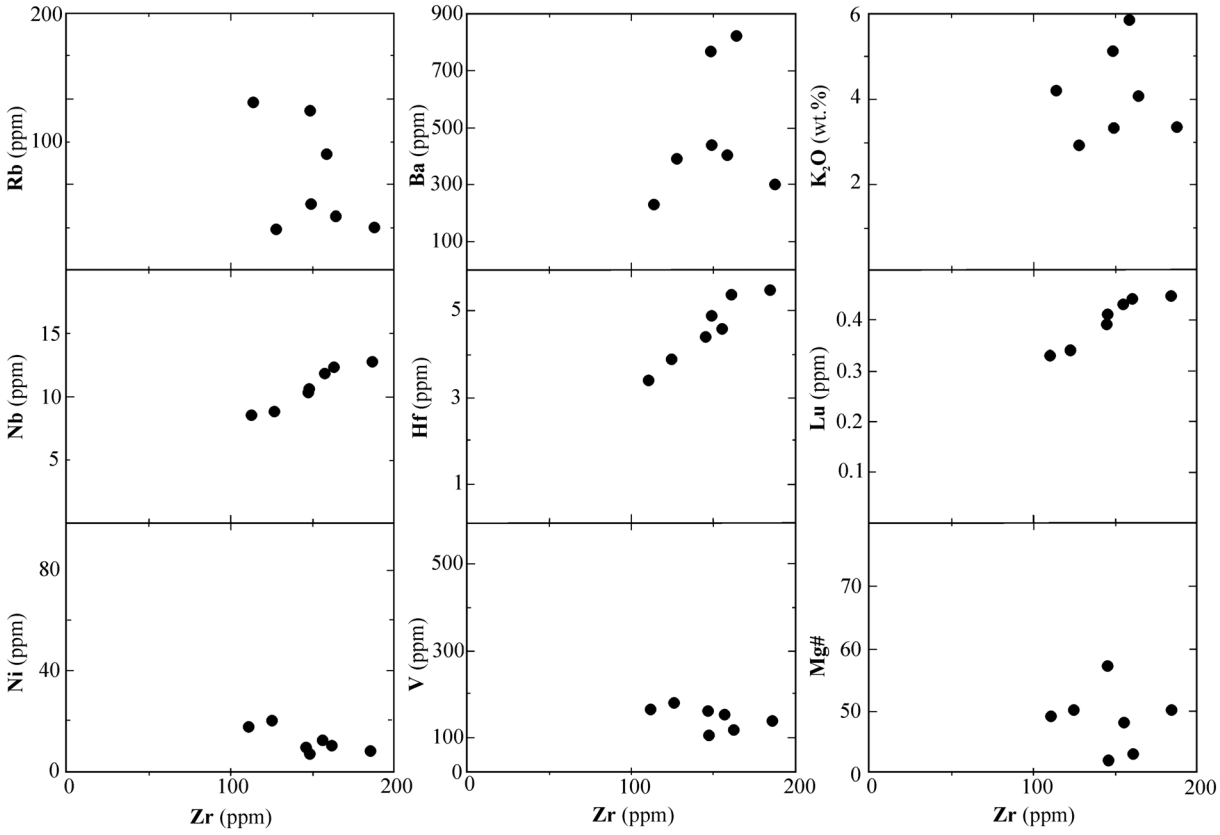

FIGURE 5 Variation diagrams for selected elements with Zr as index of differentiation for the andesitic pyroclastic rocks from Ivanščica Mt

hydrothermal activity (Ruitz-Ortiz et al., 1989). An exception from the trend makes the sample ce-34/1 whose reduced value of Si/Si + Al + Fe may be a consequence of the secondary Fe enrichment (Table 3).

The Al_2O_3 content is relatively high in all analyzed rocks (2.00 to 10.32 wt %), with the maximum reported in sample ce-28 (silicified shale). Titanium content is relatively low, spanning between 0.09 to 0.61 wt % (Table 3). It is largely controlled by the heavy mineral fraction and is correlative with alumina while the correlation with MnO and MgO is rather poor (Table 3a). The content of K_2O is high, similarly to alumina, and varies between 0.86 and 4.36 wt %. It is controlled by the mica and in lesser extent by the amount of clastic component showing a high correlation with MgO and CaO (Table 3a). Content of Fe in analyzed rocks ranges between 0.11 and 0.92 wt %, which is relatively low, ruling out the hypothesis of a hydrothermal imprint. Iron is not correlative with any other element (Table 3a). Phosphorus content is low spanning between 0.04 and 0.66 wt % which may be attributed to the dilution with silica. The amounts of CaO are inversely correlated with silica (sample ce-23; Table 3). Carbonate is largely of secondary origin and is found filling the submillimeter veins in the rock; or, alternatively, it may be found as an infill of radiolarian skeletons where it has replaced Si. Calcium is highly correlative with Mn and Mg.

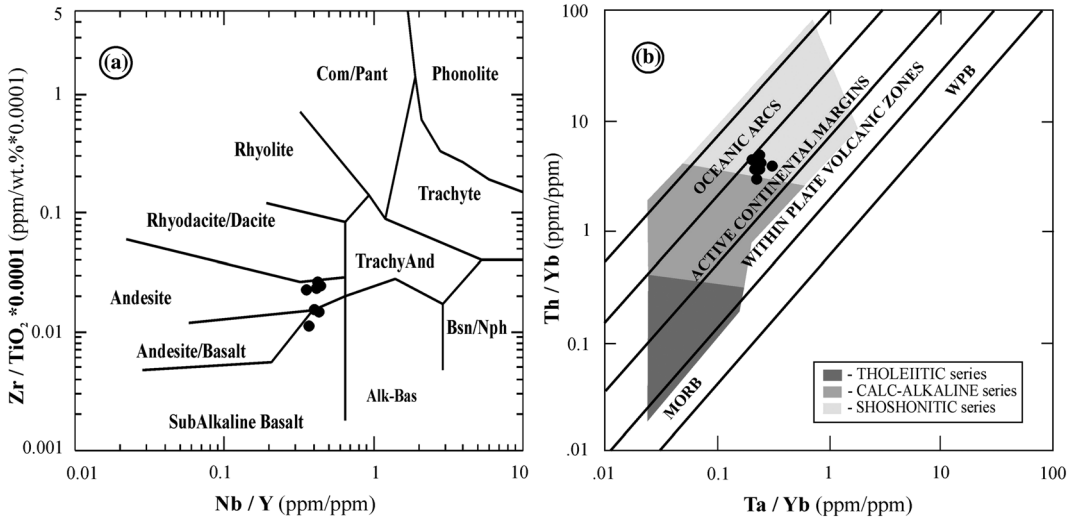

FIGURE 6 (a) Classification diagram $Zr/TiO_2 \times 0.0001$ – Nb/Y after Winchester and Floyd (1977), (b) Ta/Yb–Th/Yb discrimination diagram after Müller, Rock, and Groves (1992) and Gorton and Shandl (2000) for the andesitic pyroclastic rocks from Ivanščica Mt

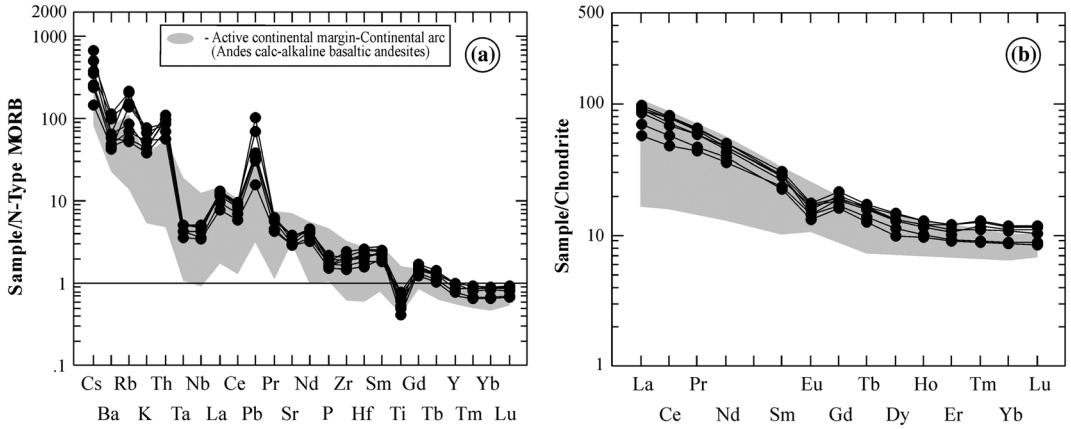

FIGURE 7 (a) N-MORB-normalized multielement and (b) REE patterns for Ivanščica Mt. andesitic pyroclastic rocks. Normalization values are from Sun and McDonough (1989). Fields for active continental margin-Continental arc calc-alkaline basaltic andesites in the Andes (Wilson, 1989) are plotted for correlation constraints

4.3 | Stratigraphy

4.3.1 | Radiolarian stratigraphy and dating

Three samples from the Cerina section were examined for radiolarians. Sample ce-26 is a dark-grey laminated chert with abundant thin-shelled bivalves (Figure 3f). The other samples (ce-32, ce-34) are dark-red chert that also contain some laminae with pelagic bivalves. Radiolarians are poorly preserved (Figures 9 and 10) and rare. In sample ce-26, long monaxon sponge spicules are associated with radiolarians. Detached spines of Oertlispongidae (Figure 9) occur in all samples and are especially abundant and diverse in the sample ce-34. Spines of *Eptingium*, Hindeosphaeridae (probably mostly *Pseudostylosphaera*), and wide tricarinate spines of *Spongoxystris* are also common but entire specimens are rare (Figure 10). *Archaeocenosphaera* and multicyrtid nassellarians (e.g., *Triassocampe*) are present in all samples. All other genera occur only sporadically (for radiolarian inventory, see Table 5).

Oertlispongidae are stratigraphically the most important. Based on the co-occurrence of *Oertlispongus inaequispinosus* Dumitrica, Kozur, and Mostler and *Baumgartneria bifurcata* Dumitrica, all three samples have been assigned to the *Spongosilicarmiger italicus* Zone as defined by Kozur and Mostler (1994) and Kozur, Krainer, and Mostler (1996). The *Spongosilicarmiger italicus* Zone has been subdivided into the lower *Oertlispongus primitivus* Subzone and the upper *Oertlispongus inaequispinosus* Subzone (Kozur et al., 1996; Kozur & Mostler, 1994). In this paper, we consider *Oertlispongus primitivus* Kozur and Mostler to be included in the variability of *Oertlispongus inaequispinosus* Dumitrica, Kozur, and Mostler (see comments on Figure 9, 13–18). Hence, we do not assign the samples to a subzone but to the zone only. The *Spongosilicarmiger italicus* Radiolarian Zone corresponds to the Upper Anisian *Reitziites reitzi* ammonoid Zone (Kozur, 2003).

TABLE 3A Spearman *R* correlation for major and trace elements for cherts from Ivanščica Mt

SiO_2	TiO_2	Al_2O_3	Fe_2O_3	MnO	MgO	CaO	Na_2O	K_2O	P_2O_5	Ba	Co	Cr	Hf	Nb	Ni	Rb	Sc	Sr	Th	V	Y	Zr	
SiO_2	1.00																						
TiO_2	−0.79	1.00																					
Al_2O_3	−0.75	0.96	1.00																				
Fe_2O_3	−0.11	0.07	0.11	1.00																			
MnO	−0.64	0.75	0.68	−0.43	1.00																		
MgO	−0.96	0.75	0.79	0.14	0.57	1.00																	
CaO	−0.86	0.71	0.68	−0.36	0.89	0.82	1.00																
Na_2O	−0.39	0.68	0.71	0.43	0.50	0.43	0.32	1.00															
K_2O	−0.82	0.68	0.71	−0.07	0.50	0.86	0.75	0.14	1.00														
P_2O_5	−0.41	0.50	0.63	−0.02	0.63	0.54	0.58	0.76	0.32	1.00													
Ba	−0.82	0.89	0.96	0.07	0.64	0.89	0.75	0.61	0.82	0.67	1.00												
Co	−0.68	0.54	0.43	0.64	0.21	0.57	0.32	0.43	0.43	0.04	0.39	1.00											
Cr	0.15	0.02	0.02	0.84	−0.58	−0.15	−0.60	0.22	−0.25	−0.36	−0.09	0.40	1.00										
Hf	−0.73	0.92	0.82	0.15	0.54	0.64	0.54	0.45	0.64	0.12	0.73	0.64	0.23	1.00									
Nb	−0.60	0.87	0.76	0.29	0.49	0.49	0.40	0.56	0.49	0.12	0.62	0.71	0.34	0.95	1.00								
Ni	−0.11	−0.04	−0.04	0.89	−0.59	0.11	−0.41	0.04	0.04	−0.39	−0.04	0.63	0.85	0.19	0.26	1.00							
Rb	−0.39	0.46	0.57	0.39	0.04	0.50	0.18	0.29	0.71	0.23	0.61	0.43	0.24	0.45	0.47	0.41	1.00						
Sc	−0.86	0.95	0.95	−0.02	0.73	0.86	0.80	0.52	0.86	0.51	0.95	0.49	−0.12	0.86	0.76	−0.06	0.58	1.00					
Sr	−0.93	0.68	0.57	0.11	0.68	0.82	0.82	0.39	0.61	0.34	0.61	0.75	−0.18	0.64	0.56	0.07	0.14	0.69	1.00				
Th	−0.75	0.96	0.93	0.11	0.61	0.71	0.61	0.57	0.64	0.34	0.86	0.50	0.16	0.95	0.87	0.07	0.43	0.92	0.61	1.00			
V	−0.50	0.43	0.54	0.75	0.11	0.61	0.21	0.75	0.32	0.61	0.57	0.61	0.36	0.26	0.33	0.48	0.54	0.41	0.43	0.36	1.00		
Y	−0.36	0.61	0.71	0.11	0.61	0.46	0.46	0.89	0.25	0.95	0.68	0.11	−0.15	0.26	0.31	−0.30	0.29	0.54	0.29	0.46	0.64	1.00	
Zr	−0.61	0.86	0.75	0.36	0.43	0.50	0.36	0.57	0.43	0.09	0.61	0.71	0.44	0.95	0.98	0.33	0.39	0.73	0.57	0.89	0.36	0.29	1.00

Note: Significant correlation at $p < .05$. −: indicates negative correlation.

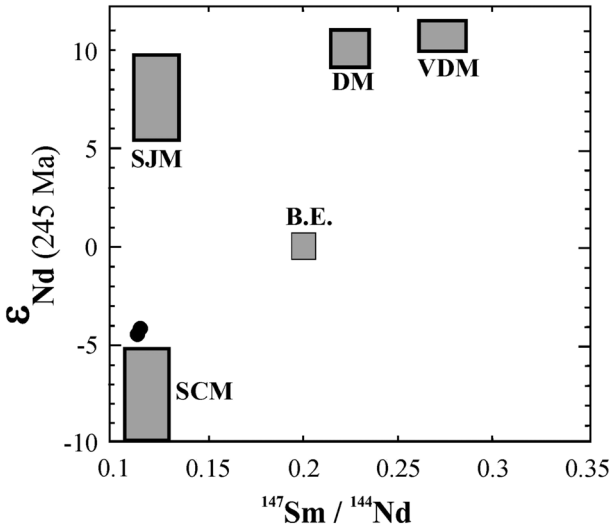

FIGURE 8 $^{147}Sm/^{144}Nd$–$\varepsilon_{Nd(245Ma)}$ diagram for the andesitic pyroclastic rocks from Ivanščica. Hypothetical mantle sources: DM = depleted mantle (not refractory), VDM = very depleted mantle (refractory), SJM = subducted juvenile material (subducted oceanic crust; slab with little pelagic sediment), and SCM = subducted continental material. The observed compositions and hypothetical end member sources calculated for the Middle Triassic following Swinden et al. (1990)

TABLE 4 Nd and Sr isotope data of andesitic pyroclastic rocks from the Mt. Ivanščica

Sample	Rock type	$^{143}Nd/^{144}Nd$[a]	$^{147}Sm/^{144}Nd$	$^{87}Sr/^{86}Sr$[a]	εNd (245 Ma)[b]	$^{87}Sr/^{86}Sr$ (245 Ma)[c]
ce-11	Andesite tuff	0.512299 (4)	0.115514	0.707562 (10)	−4.18	0.706217
ce-16	Andesite tuff	0.512282 (7)	0.113175	0.707523 (11)	−4.44	0.703745

[a]Errors in brackets for Nd and Sr isotopic ratios are given at the 2σ level. $^{147}Sm/^{144}Nd$ calculated from the ICP-MS concentrations of Sm and Nd following equation: $^{147}Sm/^{144}Nd = (Sm/Nd) \times (0.53151 + 0.14252 \times {}^{143}Sm/^{144}Nd)$.

[b]Initial εNd (245 Ma) calculated assuming $I^oCHUR = 0.512638$, $(^{147}Sm/^{144}Nd)^oCHUR = 0.1966$, and $\lambda Sm = 6.54*10^{-12}a^{-1}$.

[c]$^{87}Sr/^{86}Sr$(245 Ma) calculated using ICP-MS Rb and Sr concentrations and assuming $\lambda Rb = 1.42 \times 10^{-11}a^{-1}$.

5 | DISCUSSION

Geological and geochemical characteristics of Ivanščica Mt. pyroclastic, siliciclastic, and siliceous rocks are in favour of the existence of a volcano-sedimentary succession, which testifies an intensive and explosive volcanic activity. The succession also makes a record of radiolarian chert deposition in relatively deep-water environment. The biostratigraphic age based on radiolarians (Figure 2, 9, and 10) is Late Anisian which is in accordance with previously known data on Ivanščica Mt. Highly similar radiolarian assemblages were described by Goričan et al. (2005) from two lithologically comparable sections in the Belski dol quarry, which is located in vicinity, only 1-km north of the Cerina section (Figure 1c). Published prior the GSSP for the Ladinian Stage was formally established at the base of the *Eoprotrachyceras curionii* Ammonoid Zone (Brack, Rieber, Nicora, & Mundil, 2005), we hereby note that Goričan et al. (2005) consider the *Reitziites reitzi* Ammonoid Zone to be the lowermost zone of the Ladinian. The Early Ladinian radiolarian ages originally proposed for the Belski dol and other sections in NW Croatia (Goričan et al., 2005) should thus be shifted to Late Anisian.

5.1 | Mineralogical, petrogenetic, and tectonomagmatic significance

5.1.1 | Pyroclastic rocks

Analyzed tuffs of Ivanščica Mt. originated from a moderately viscous andesitic magma through a series of explosive volcanic eruptions which is indicated by irregularly shaped volcanic shards (Leyrit & Montenat, 2000; Figure 2c) and their mineral composition (Figure 2–4). Such explosions are commonly linked to the volcanos formed at the top of subduction zones (e.g., Frisch, Meschede, & Blakey, 2011 and references therein; Sottli, Palladino, Cuffaro, & Doglioni, 2015). A report on lithoclasts of andesite lava present in the lower portion of the Cerina section as well as a general grain size decrease up section, indicates a gradual decline in the intensity of volcanic activity accompanied by the deposition of fine-grained tuffs in the upper portion of the volcanoclastic package. During the duration of tuff accumulation, there were, however, at least two phases of high-intensity volcanism manifested by the occurrence of coarse-grained tuff varieties in the middle portion of the section (samples ce-14 through ce-17; Figure 2/III) and in the one positioned higher

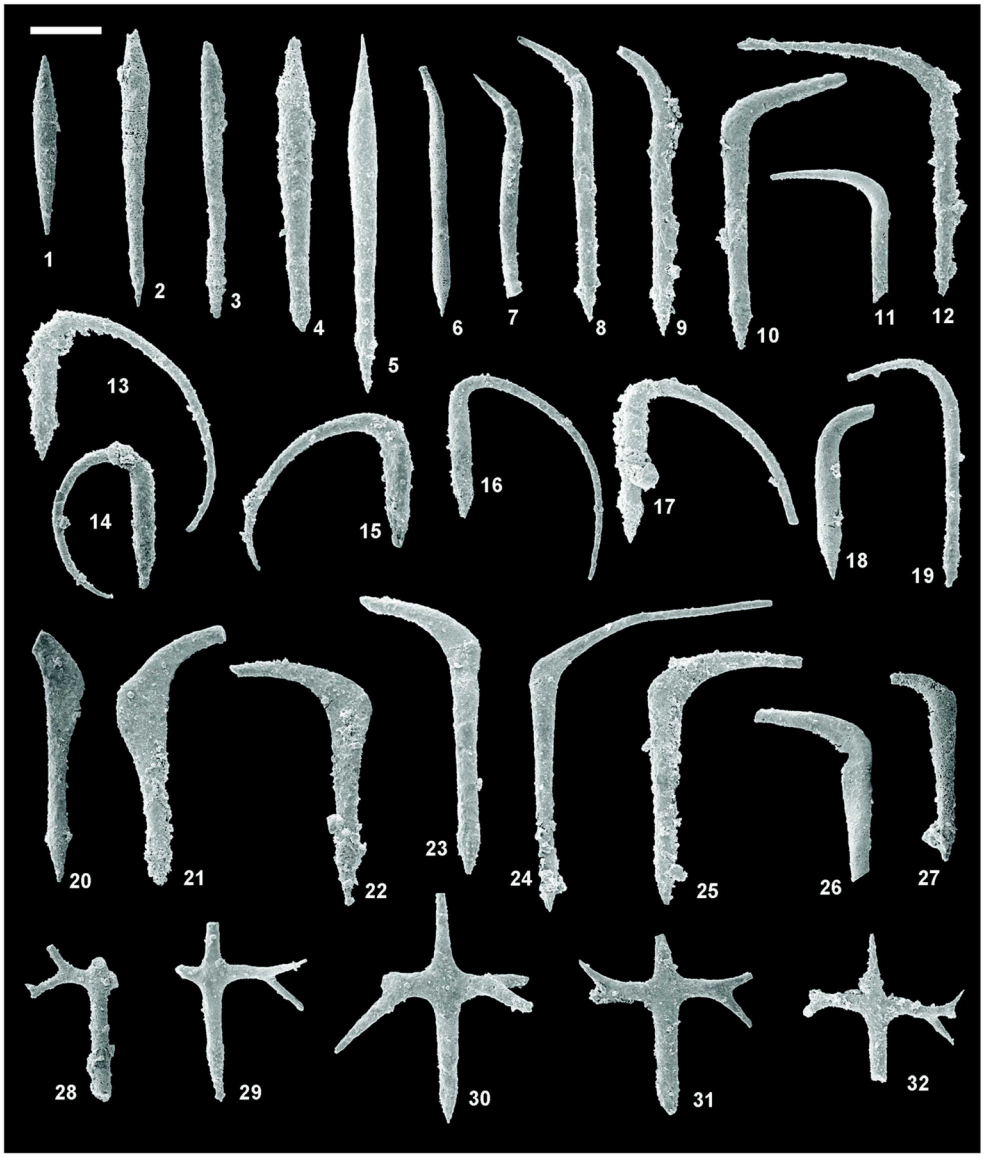

FIGURE 9 Spines of Oertlispongidae. Length of scale bar 100 μm for all illustrations. For each specimen, sample number is indicated. Taxonomic remarks are given where necessary. 1. *Paroertlispongus*? sp. 1 sensu Dumitrica (1999). 1: ce-26. This spine differs from the spine of *Paroertlispongus multispinosus* Kozur and Mostler by being shorter, proportionally wider and by having the widest part not distally but near the middle of the spine. 2–5. *Paroertlispongus multispinosus* Kozur and Mostler. 2: ce-26; 3: ce-32; 4–5: ce-34. 6–9. *Paroertlispongus weddigei* (Lahm). 6: ce-26; 7: ce-32; 8–9: ce-34. Spines with variously bent short distal part are included. The angle of the bending is 45 ° or less. *Pseudoertlispongusmostleri* Kozuris considered synonym of *Paroertlispongusweddigei*. 10–12. *Oertlispongus primus* Kozur. 10: ce-34; 11: ce-32; 12: ce-34. 13–18. *Oertlispongus inaequispinosus* Dumitrica, Kozur and Mostler. 13–17: ce–34; 18: ce-26. Based on the height of the stem and the degree of distal curving, Kozur and Mostler (1994) distinguished several subspecies of *O. inaequispinosus* and introduced two new species *Oertlispongus primitivus* and *Oertlispongus aspinosus*. One of the subspecies, *O. inaequispinosus tumidospinosus* Kozur and Mostler, was later raised to species level (Dumitrica, 1999). Because of the gradualism among different shapes (compare Figure 13–17 from sample ce–34) and because the differentiation is not possible in incomplete spines (Figure 18), we herein assign all these morphotypes to *O. inaequispinosus*. We note however, that in all specimens from the ce section the stem is longer than the diameter of the shell. According to Kozur and Mostler (1994), such relatively long stems are characteristic of stratigraphically older *Oertlispongus*. 19. *Oertlispongus* aff. *inaequispinosus* Dumitrica, Kozur and Mostler, ce-34. This spine with a long stem and a short down-curved distal part represents an intermediate morphotype between *Oertlispongus primus* and *Oertlispongus inaequispinosus*. We found only one specimen in sample ce-34, which also contains the other two species. 20–27. *Falcispongus falciformis* Dumitrica. 20: ce-26; 21–25: ce-34; 26: ce-32; 27: ce-26. We follow the original definition by Dumitrica (1982) who determined *F. falciformis* with a great variability in the width of wings. In our material, a continuum of very narrow to rather wide wings has been observed in a single sample (see Figure 21–25 from sample ce-34). *F. praefalciformis* Kozur and Mostler and *F. zapfei* Kozur are herein considered synonyms of *F. falciformis*. 28–31. *Baumgartneria bifurcata* Dumitrica. 26: ce-26; 29: ce-32; 30–31: ce-34. The lateral branches of these spines are bifurcate but more straight and shorter than in typical *Baumgartneria bifurcata*. The overall shape, except for the bifurcating spine tips, is the same as in *Baumgartneria trifurcata*. 32. *Baumgartneria trifurcata* Dumitrica, ce-34. [Correction added on 3 December 2019, after first online publication: The legend for Figure 9 has been corrected.] [Colour figure can be viewed at wileyonlinelibrary.com]

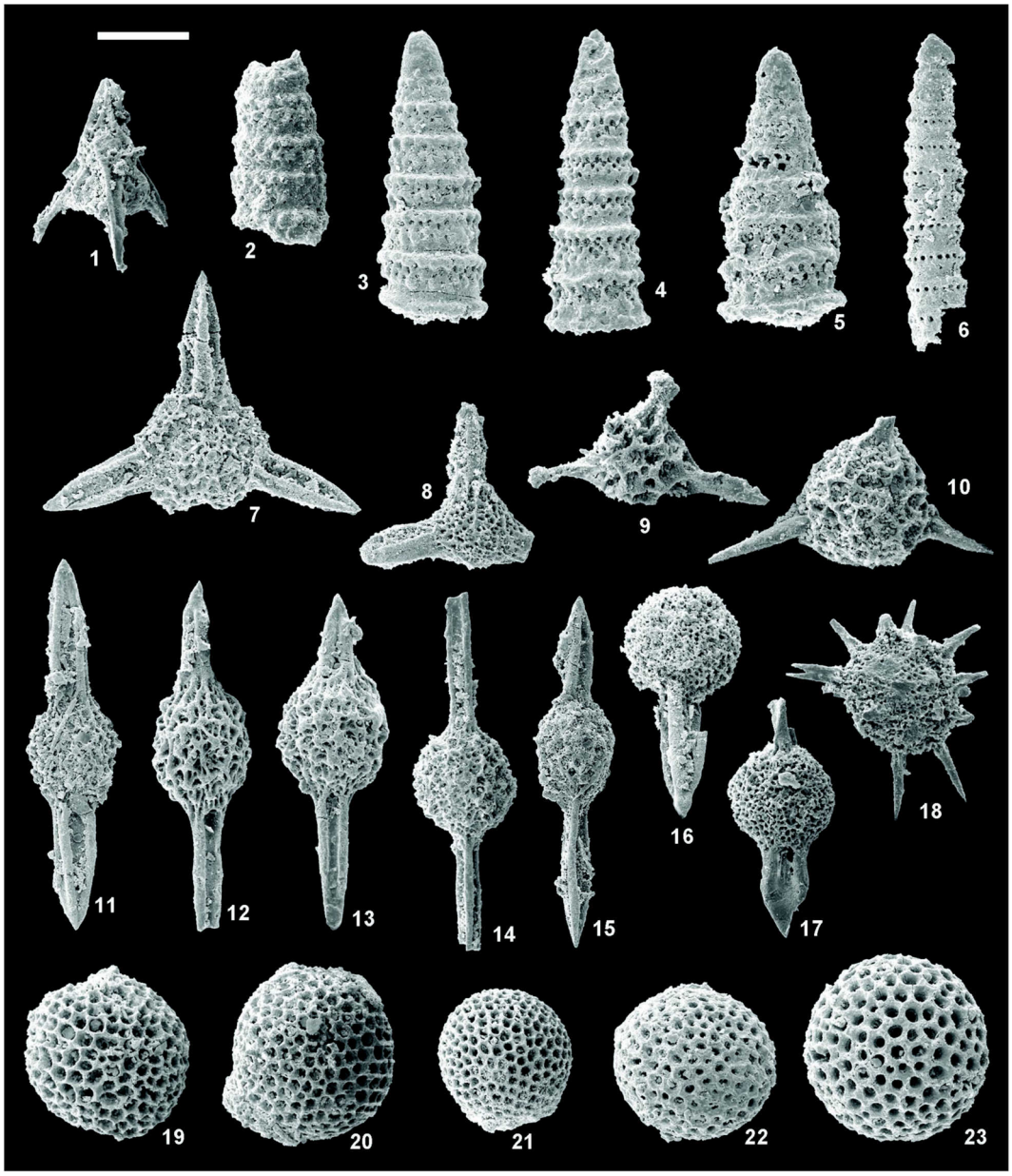

FIGURE 10 Other radiolarians. Sample number and length of scalebar are indicated for each specimen. 1. *Hinedorcus fassanicus* (Kozur), ce-32, scale bar 75 μm. 2–3. *Triassocampe scalaris* Dumitrica, Kozur and Mostler. 2: ce-26; 3: ce-34, scale bar 75 μm. 4–5. *Triassocampe deweveri* (Nakaseko and Nishimura), ce-34, scale bar 75 μm. 6. *Annulotriassocampe campanilis* Kozur and Mostler, ce-32, scale bar 75 μm. 7. *Eptingium nakasekoi* Kozur and Mostler, ce-34, scale bar 100 μm. 8. *Triassistephanidium laticorne* Dumitrica, ce-32, scale bar 100 μm. 9. *Cryptostephanidium cornigerum* Dumitrica, ce-32, scale bar 75 μm. 10. *Spongostephanidium spongiosum* Dumitrica, ce-32, scale bar 75 μm. 11. *Pseudostylosphaera canaliculata* (Bragin), ce-34, scale bar 150 μm. 12–13. *Pseudostylosphaera* aff. *tenuis* (Nakaseko and Nishimura), ce-34, scale bar 100 μm. The spines are thicker than in typical *P. tenuis*. 14. *Pseudostylosphaera longispinosa* Kozur and Mostler, ce-32, scale bar 100 μm. 15. *Pseudostylosphaera postjaponica* Kozur and Mostler, ce-34, scale bar 150 μm. 16. *Spongoxystris tetraptera* (Ramovš and Goričan), ce-32, scale bar 100 μm. 17. *Spongoxystris* sp., ce-32, scale bar 100 μm. 18. *Triassospongosphaera multispinosa* (Kozur and Mostler), ce-32, scale bar 100 μm. 19–23. *Archaeocenosphaera* spp. 19–20: ce-26; 21: ce-32; 22–23: ce-34; scale bar 100 μm. [Correction added on 3 December 2019, after first online publication: The legend for Figure 10 has been corrected.] [Colour figure can be viewed at wileyonlinelibrary.com]

in the section within the lower chert series (samples ce-28 and ce-33; Figure 2/V).

The Cerina section pyroclastites are characterized by a variety of inclusions merged in a palagonitized and altered glassy matrix. The inclusions are represented by plagioclase and K-feldspar as well as ferromagnesian minerals. All primary silicates are occasionally pseudomorphed by secondary sericite, chlorite, Fe-Mg-rich clay minerals, and calcite. The fine-grained matrix, which dominates analyzed rocks, is chiefly consisted of altered volcanic glass affected by an advanced palagonitization and diagenesis. The lower portion of the section is rich in illite–smectite, chlorite, and Fe-rich mica. On the other hand, in the middle portion of the section matrix is essentially

TABLE 5 Occurrence of radiolarian species in samples from the Cerina section

Species	Samples		
	ce-26	ce-32	ce-34
Oertlispongidae			
Baumgartneria bifurcata Dumitrica	x	x	x
Baumgartneria trifurcata Dumitrica			x
Falcispongus falciformis Dumitrica	x	x	x
Oertlispongus inaequispinosus Dumitrica, Kozur, and Mostler	x	x	x
Oertlispongus aff. *inaequispinosus* Dumitrica, Kozur, and Mostler			x
Oertlispongus primus Kozur		x	x
Paroertlispongus multispinosus Kozur and Mostler	x	x	x
Paroertlispongus weddigei (Lahm)	x	x	x
Paroertlispongus? sp. 1 sensu Dumitrica, 1999	x		
Other Spumellaria			
Archaeocenosphaera spp.	x	x	x
Spongoxystris tetraptera (Ramovš and Goričan)		x	
Spongoxystris spp. with tricarinate spines (mostly detached spines)		x	x
Triassospongosphaera multispinosa (Kozur and Mostler)		x	
Entactinaria			
Pseudostylosphaera canaliculata (Bragin)			x
Pseudostylosphaera longispinosa Kozur and Mostler		x	
Pseudostylosphaera postjaponica Kozur and Mostler			x
Pseudostylosphaera aff. *tenuis* (Nakaseko and Nishimura)		x	x
Cryptostephanidium cornigerum Dumitrica		x	
Eptingium nakasekoi Kozur and Mostler			x
Spongostephanidium spongiosum Dumitrica		x	
Triassistephanidium laticorne Dumitrica		x	x
Nassellaria			
Hinedorcus fassanicus (Kozur)		x	
Annulotriassocampe campanilis Kozur and Mostler		x	
Triassocampe deweveri (Nakaseko and Nishimura)			x
Triassocampe scalaris Dumitrica, Kozur, and Mostler	x		x

consisted of the two distinct smectite varieties, nontronite and montmorillonite–beidelite. Finally, the upper portion of the section contains well-preserved glass fragments with a myriad of unaltered laths of plagioclase. There, no discrete smectite has been reported which is in line with a lower degree of alteration in the upper part of the section. Different alteration assemblages detected are thought to reflect the variations in eogenetic fluid composition and extent of fluid circulation. More specifically, the dominance of expandable clay species (smectite and illite–smectite) in the lower and middle portion of the column must have resulted from an extensive in situ eogenesis of coarse-ash sized and permeable pyroclastic material, which led to clay mineral formation in an open hydrologic system (e.g., Christidis & Huff, 2009; Šegvić et al., 2014; Zhao et al., 2017). This conforms to the general up-section grain size decrease reported herein. Further on, an oxygenated eogenetic environment may be hypothesized with most of leached Fe taken by the neoformed ferric smectite that dominates the middle part of the section (e.g., Christidis, 1998). The alteration of volcanic material that leads to smectite formation normally involves an in situ hydrolysis in marine, brackish, fresh water, or hydrothermal fluids (Chamley, 1989; Velde, 1995), while the large water-to-rock ratio of an open system favours smectite mineralization regardless of the composition of the parent volcanic rock (Christidis & Huff, 2009). On the other hand, lack of smectite in the tuffs from the upper section of the column as well as the preservation of volcanoclastic component calls for somewhat restricted degrees of water percolation, presumably as a result of an enhanced compaction of the pristine volcanic material along with environmental changes during sedimentation of volcanic ash. Another line of evidence in favour of these developments is the presence of yellowish palagonite (Figures 3b and 4b), which normally marks incipient diagenetic stages (Bishop, Schiffman, & Southard, 2002; Singer, 1974) defined by water penetration, which, in the case of analyzed tuffs, gave rise to glass

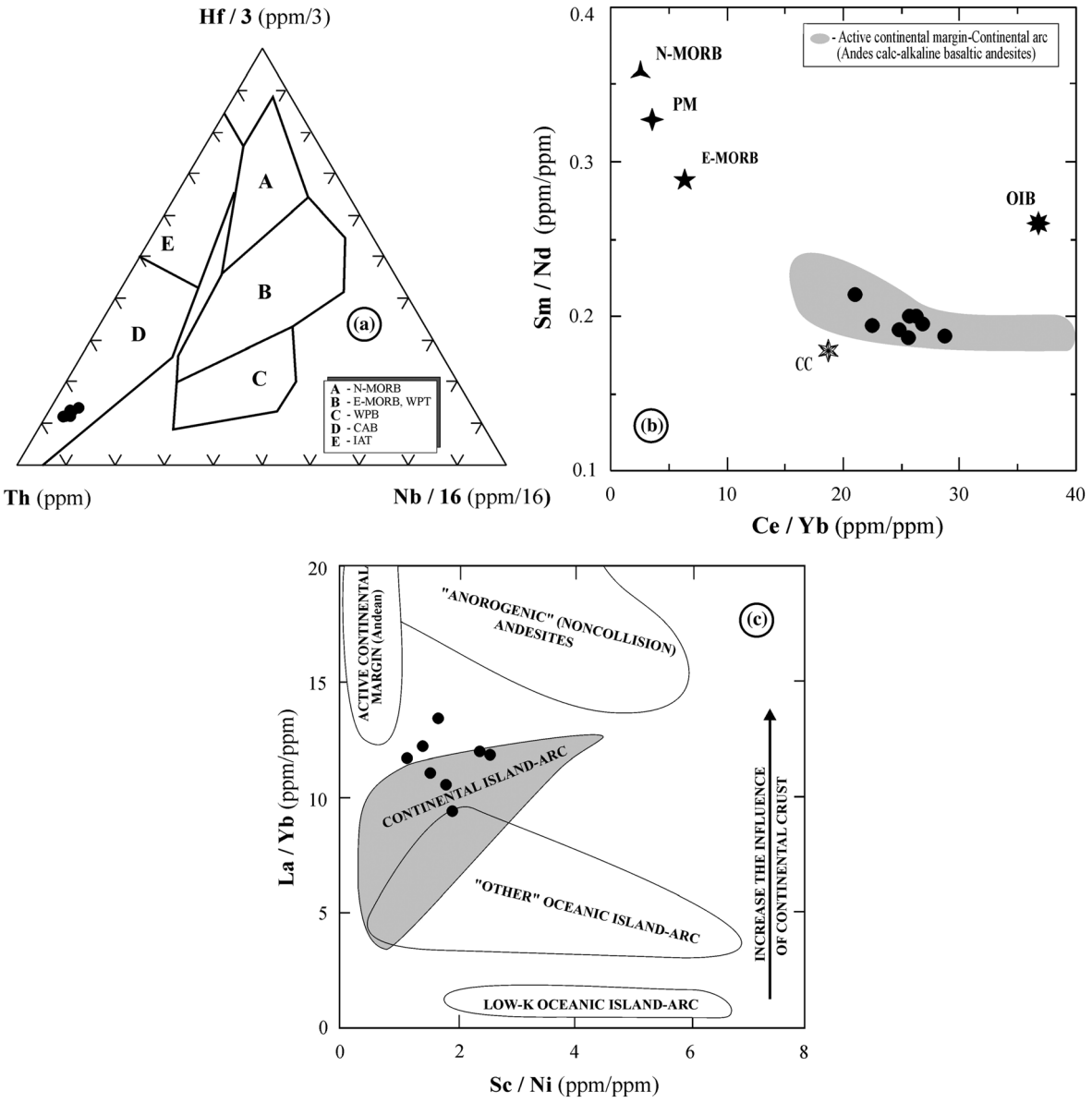

FIGURE 11 Discrimination diagrams for the andesitic pyroclastic rocks from Ivanščica Mt. (a) Th–Nb/16–Hf/3 diagram (Wood, 1980). Abbreviations: A = normal mid-ocean ridge basalts (N-MORB); B = enriched MORB (E-MORB) and within-plate tholeiites (WPT); C = alkaline within-plate basalts (AWPB); D = calc-alkali basalts (CAB); E = island-arc tholeiites (IAT). (b) Ce/Yb–Sm/Nd diagram. Fields for N-MORB, E-MORB, PM (Primitive mantle) and OIB are from Sun and McDonough (1989), CC (Continental crust) is from Rudnick and Fountain (1995) and Active continental margin-Continental arc is from Wilson (1989). (c) Sc/Ni–La/Yb diagram (after Bailey, 1981)

hydration and neoformation of micro to cryptocrystalline phyllosilicates from the illite–alumoceladonite series. Finally, the deep diagenetic obliterations of argillic tuffs of the Cerina section may be excluded, taking into account an overall thickness of the tuff hosting lower Triassic sedimentary succession (400–750 m) and a lack of directly superimposed younger deposits (Šimunić, 1992; Šimunić et al., 1982).

Andesite and basalt tuffs of Ivanščica Mt. show uniform and yet complex geochemical signatures, which is in line with their diverse genesis. In the Hf/3-Th-Nb/16 discrimination diagram (Figure 11a), the tuffs are plotted within the orogeny field, characteristic for calc-alkaline arc-related volcanic rocks, which suggests a subduction-related nascent environment of these rocks. Highly calc-alkaline to shoshonitic character is a typical geochemical characteristic of mature volcanic arcs (e.g., Wilson, 1989). Enrichment in LILE, Th, and LREE concentrations and negative anomalies of Nb-Ta, P, and Ti (Figure 7), along with the depletion in HFS elements, are also the characteristics of subduction-related magmas and are commonly attributed to a mantle source that was modified by metasomatic hydrous fluids and melts derived from the subduction slab (e.g., Elburg et al., 2002; Hawkesworth, Gallagher, Hergt, & McDermott, 1993; Hawkesworth, Turner, McDermott, Peate, & Van Calsteren, 1997; Pearce, 1983). This unambiguously suggests the presence of the ancient-subducted oceanic crust of Palaeotethys that had a decisive influence on the formation of Ivanščica Mt. pyroclastic rocks during Late Anisian. Similar conclusions were reached by Pe-Piper (1998) who studied Triassic volcanic rocks in the Hellenides, suggesting an earlier Hercynian subduction event that gave rise to the Andean-

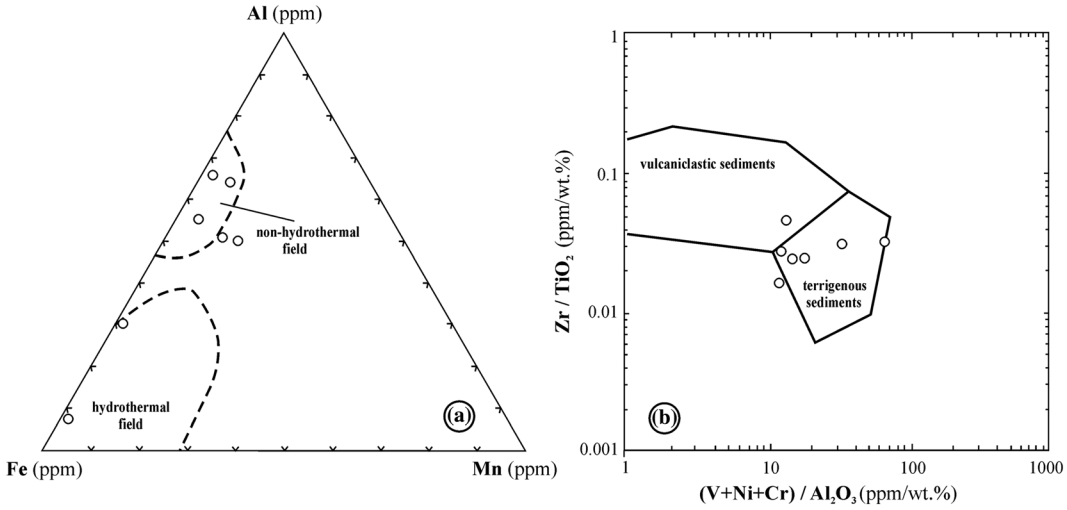

FIGURE 12 Discrimination diagrams for the cherts from Ivanščica Mt. (a) Fe–Al–Mn diagram (Adachi et al., 1986). (b) Zr/TiO_2–$(V+Ni+Cr)/Al_2O_3$ diagram (Andreozzi et al., 1997)

type arc on the northeastern margin of Gondwana. High values of Th/La (0.31–0.49), Th/Yb (3.84–4.82), Th/Ta (14.2–20.6), and La/Nb (2.4–3.4) and pronounced positive Pb spikes (up to 11.2; Figure 7a), which are sensitive indicators of crustal contamination (e.g., Taylor & McLennan, 1985), may connote an intensive chemical interaction of analyzed tuffs of Ivanščica Mt. with the continental crust; whereby, the latter must have played a role in the genesis of the former. This is corroborated by the negative values of initial ε_{Nd} (−4.18 to −4.44) accompanied by the very low values of $^{147}Sm/^{144}Nd$ ratio (≤0.113175; Figure 8). Conspicuous contamination by continental component may be a result of slow and long magma uplift through the continental crust (e.g., Huppert & Stephen, 1985; Pomonis, Tsikouras, & Hatzipanagiotou, 2004). Further constrains on a complex genesis of analyzed tuffs may be invoked by interpreting the Th/Yb versus Ta/Yb, Sm/Nd versus Ce/Yb, and La/Yb versus Sc/Ni discrimination diagrams (Figures 6b and 11b,c), as well as the spider and REE normalization diagrams (Figure 7). Considering a calc-alkaline to shoshonitic character of analyzed tuffs, the listed discrimination criteria clearly support the origin of Ivanščica Mt. pyroclastic rocks in an ensialic mature volcanic arc setting that developed in an active continental margin environment analogue to the Andean-type volcanism.

One may hypothesize, based on the presented geochemical and isotopic data assemblage, that the andesite and basalt tuffs of Ivanščica Mt. were derived by partial melting of the subcontinental lithospheric mantle that had been metasomatized already in mantle wedge by LILE-enriched hydrous fluids and melts derived from subducted sediments. These early subduction-related processes might have therefore had an impact on lithospheric mantle leaving an imprint in the geochemistry of analyzed tuffs. Andesitic melts erupted through the tectonically weakened zones of upper crust were henceforth contaminated by crustal components. Lastly, in addition to partial melting, the genesis of analyzed tuff must have included a fractional crystallization indicated by relatively low MgO/FeO_{tot} ratios (0.42–0.57) coupled with very low-to-low abundance of Ni and Cr (5.4–20 ppm and 28–103 ppm, respectively).

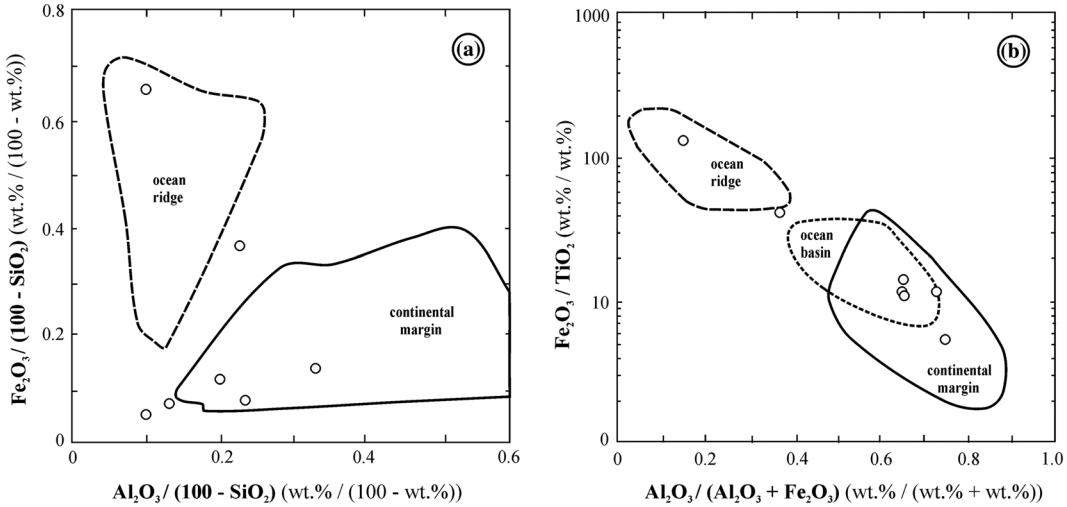

FIGURE 13 Discrimination diagrams for the cherts from Ivanščica Mt. (a) $Al_2O_3/(SiO2)$–$Fe_2O_3/(100\text{-}SiO_2)$ diagram (Murray, 1994). (b) $Al_2O_3/(Al_2O_3+Fe_2O_3)$–$Fe_2O_3/TiO_2$ diagram (Murray, 1994)

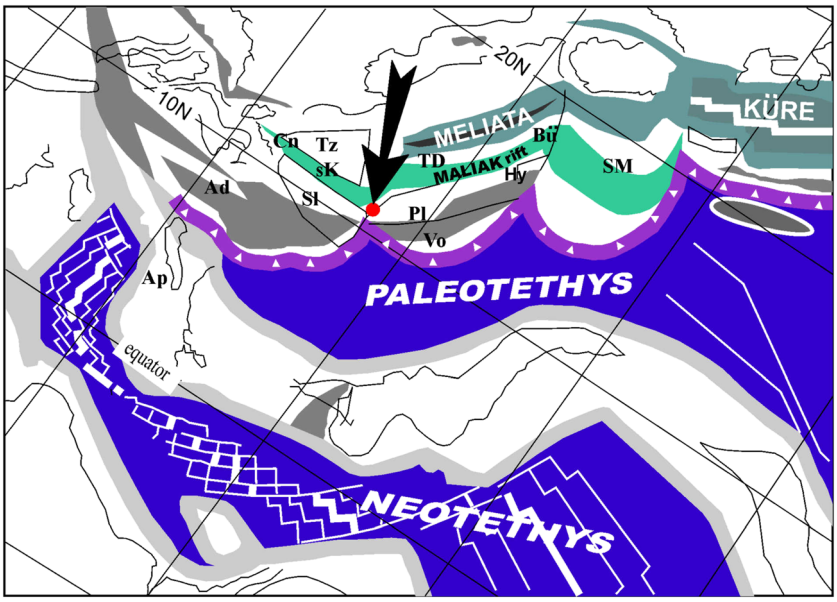

FIGURE 14 The Anisian (240 Ma) palaeogeographic reconstruction (simplified after Stampfli & Borel, 2004 with location of investigation area of Ivanščica Mt. (marked with black arrow and dot symbol). Abbreviations for neighbouring terranes: Ad = Adria s. str., Ap = Apulia s. str., Bü = Bükk, Cn = Carnic-Julian, Hy = Hydra, Pl = Pelagonian, sK = south-Karawanken fore arc, Sl = Slavonia, SM = Serbo-Macedonian, TD = Trans-Danubian, Tz = Tisza, Vo = Vourinos (Pindos) [Colour figure can be viewed at wileyonlinelibrary.com]

5.1.2 | Sedimentary rocks

On the example of the Triassic and Jurassic cherts of central Japan as well as from the deep cores of the Pacific Ocean (DSDP), Sugisaki, Yamamoto, and Adachi (1982) and Adachi, Yamamoto, and Sugisaki (1986) suggested that Mn content of siliceous rocks may serve as a good indicator of hydrothermal influence while the Ti content points out the impact of terrigenous component. The diagenesis may lead to Mn depletion in cherts as suggested by Murray (1994); and yet, the studies of Kunimaru, Shimizu, Takahashi, and Yabuki (1998) and Shimizu, Kunimaru, Yoneda, and Adachi (2001) have demonstrated the potential of Mn as a provenance indicator.

In the ternary diagram Fe–Al–Mn (Figure 12a; Adachi et al., 1986), five samples from the Cerina section has been projected within the nonhydrothermal field while two samples (ce-31 and ce-34/1) are found in the hydrothermal field. This indicates an overwhelming influence of terrigenous input at the time of sediment deposition. We suggest a stable depositional setting that remained unaltered even during the deposition of the two samples projected in the hydrothermal field. This is strongly advocated by the nature of sample ce-36 (positioned higher in the section relative to hydrothermal samples), which is found in a nonhydrothermal field. The two samples of hydrothermal nature are found in the vicinity of tuffaceous interlayers, which may have served as a source of elemental contamination (Fe and Mn) of chert during diagenesis.

Analogue results are inferred using the Al/Al + Fe + Mn ratio (Table 3). Values that equal or exceed 0.6 are indicative for terrigenous input, while the lower values of mentioned ratio are characteristic for hydrothermal influence (Baltuck, 1982; Ruitz-Ortiz et al., 1989). Five analyzed samples (ce-21, ce-23, ce-26, ce-28, and ce-36) have the mean Al/Al + Fe + Mn value of 0.66, while two samples (ce-31 and ce-34/1) have the values of around 0.20. Such depleted amounts may be explained by the diagenetic mobilization of Fe and Mn from tuffaceous interlayers. High terrigenous influence during chert sedimentation is further corroborated by significant correlation of trace elements (Zr, Hf, Th, Rb, Sc, and Nb; Table 3) which are strong indicators of terrigenous influence in the rock (Murray et al., 1991).

To assess the input of terrigenous material with regard to the one provenancing from the volcanoclastic source, the diagram Zr/TiO_2 versus $(V + Ni + Cr)/Al_2O_3$ (Andreozzi et al., 1997) has been utilized (Figure 12b). Sample projections show the strong terrigenous provenance somewhat influenced by the volcanoclastic component, which reflects a constant volcanic activity during the period of chert sedimentation.

The values of Al_2O_3/TiO_2 that exceed 20 or are found between ~19 and ~28 are, according to Girty, Ridge, Knaack, Johnson, and Al-Riyami (1996), characteristic for the rocks of andesitic and rhyodacitic composition, respectively, provenancing from the upper continental crust. This ratio in analyzed rocks spans from 15.72 to 30.59 (mean value 23.15), which is similar to the values reported by Girty et al. (1996), pointing out to the upper crust as a liable source of terrigenous contamination in cherts.

Aluminum, Ti, and Fe are presumably less mobile during diagenetic fractionations and are therefore suitable discrimination parameters in determination of depositional environment (Murray, 1994). By analyzing the diagrams in Figure 13, one may infer that studied rocks were deposited at the rim of the continental margin in a transition zone toward an oceanic basin. The samples ce-34 and ce-34/1 are found in or next to the ocean ridge field. This is likely a result of the mobilization of Fe and Mn during diagenesis.

Sugisaki et al. (1982), Kunimaru et al. (1998), and Shimizu et al. (2001) have however reported that the MnO/TiO_2 values inferior to 0.5 correspond to the sediment deposited at the continental shelf, continental slope, marginal sea, and areas in the vicinity of mafic rocks. Conversely, the values that exceed 0.5 are characteristic for deep oceans, tranches, and sediments of basaltic plateaus. The MnO/TiO_2 values in analyzed rocks strongly surpass the 0.5 threshold thus implying a deposition of chert in such environments.

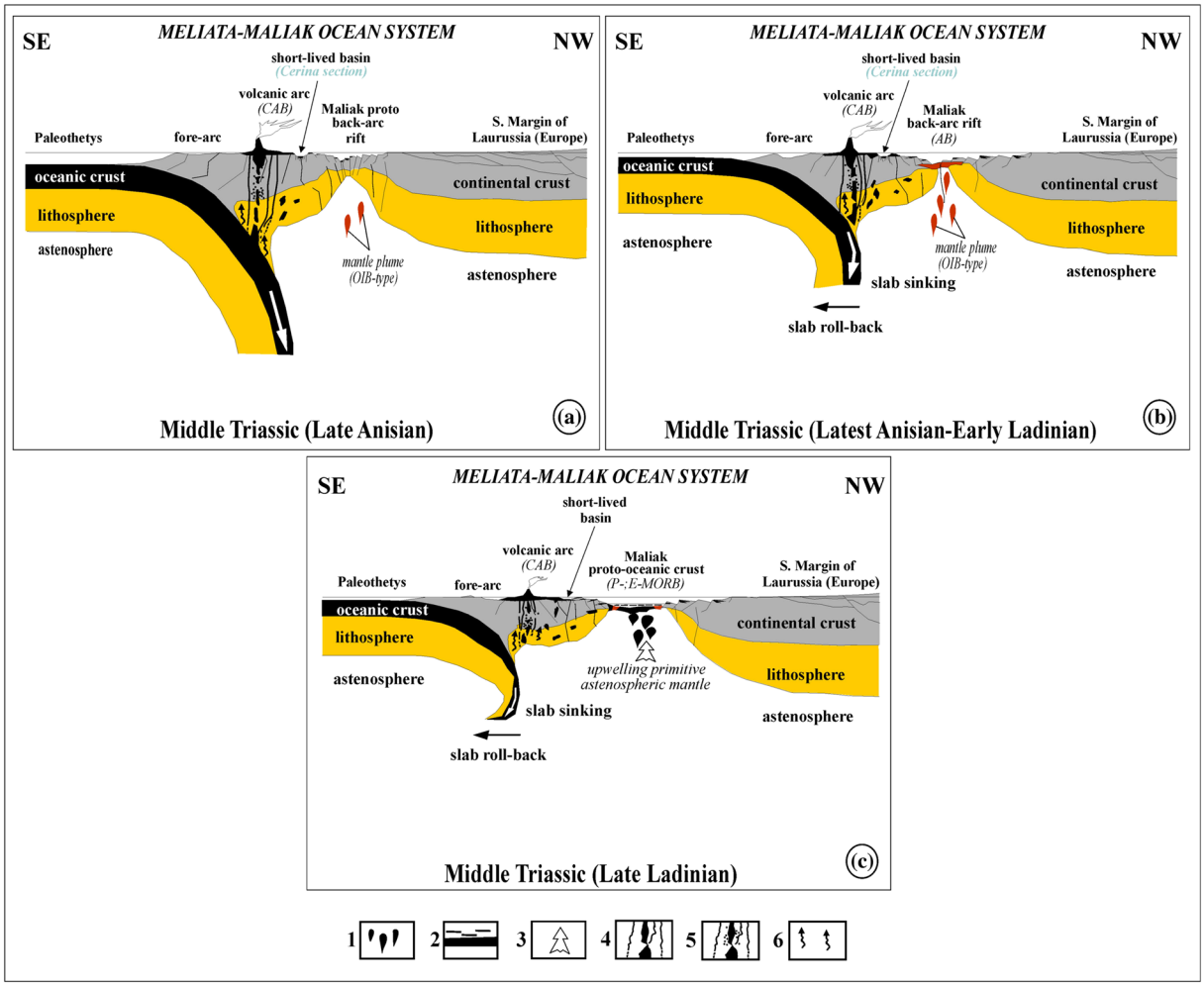

FIGURE 15 Schematic geodynamic evolutionary model for interaction of active continental margin magmatic activity, back-arc rifting and active drifting to spreading in Meliata-Maliak ocean system. Scale is approximate. (a) subduction-related ensialic volcanic arc magmatism on the active continental margin (Andean type volcanism) and roughly contemporaneous proto back-arc rifting, (b) back-arc rifting and (c) initial drifting to spreading of proto-oceanic domain. Abbreviations: CAB = calc-alkaline and shoshonitic basalt/volcanoclastite, AB = alkaline basalt, OIB = ocean island basalt, P-MORB = plume mid-ocean ridge basalt, E-MORB = enriched mid-ocean ridge basalt; 1 = mantle diapire, 2 = oceanic crust topped by radiolarian chert, 3 = raising mantle diapir, 4 = partially melted subducted oceanic lithosphere, 5 = zone of partial melting and contamination by continental crust, 6 = fluids from subducted slab [Colour figure can be viewed at wileyonlinelibrary.com]

On the other hand, the continental setting of the Cerina section is strongly suggested by the comparison with fully developed successions outcropping in the area. In the nearby Belski dol quarry (Goričan et al., 2005; Figure 1c), the correlative volcaniclastic rocks and cherts occur on top of platform carbonates and carbonate breccias and are indubitably pertained to the rifted and subsided continental margins. Another argument in favour of the continental depositional setting is a relative abundance of thin-shelled bivalves in chert layers. Such microfacies is typical of continental-shelf Upper Anisian–Lower Ladinian cherts whereas coeval oceanic ribbon cherts are devoid of pelagic bivalves (Gawlick et al., 2016).

5.2 | Geodynamic model

The northward subduction of Palaeotethyan lithosphere beneath the southern European (Laurussia) active continental margin commenced in Early Permian and continued into Early and Middle Triassic due to the movement of the Cimmerian block to the northeast (e.g., Stampfli & Borel, 2002, 2004; Schmid et al., 2008; Stampfli, Hochard, Vérard, Wilhem, & von Raumer, 2013; Figure 14). The subduction process had a great influence on the composition of mid-Triassic magmas that gave rise to the volcanic and volcanoclastic rocks of the western part of Palaeotethys (internal and external Dinarides, Southern Alps, Transdanubian region, and Bükk Mts.; Bébien et al., 1978; Castellarin et al., 1980; Castellarin et al., 1988; Obenholzner, 1991; Harangi et al., 1996; Trubelja et al., 2004; Smirčić, 2017). The Late Anisian period along the northwestern rim of the Palaeotethys is marked by the transgression linked to tectonic movements and a large-scale subsidence of the parts of carbonate platform. This had led to the formation of subduction-related ensialic arc and, then, a range of smaller intracontinental shallow (several hundred metres) short-lived sedimentary basins at the carbonate platform continental rims. Depending on bathymetry and prevailing depositional conditions, these basins were featured by the deposition

of siliciclastic, carbonate, and volcanoclastic sediments (e.g., Goričan et al., 2005; Haas et al., 2010; Figures 14 and 15a).

Such arc-related explosive magmatism present at the active continental margin yielded the Andean-type Calc-alkaline intermediate to acidic volcanoclastites and, at a lesser extent, volcanic rocks (e.g., Castellarin et al., 1988; Goričan et al., 2005). Calc-alkaline volcanism is largely shoshonitic, which also holds true for analyzed rocks of the Ivanščica Mt. that are invoked to have been formed along a destructive plate margin as a result of the subduction of oceanic lithosphere of Palaeotethys (Figure 15a,b). The volcanism is furthermore featured by inherited geochemical signatures of the Palaeotethyan subducted plate. The magmas generated in such an environment are of complex origin. The geotectonic and petrogenetic model of their formation includes the processes of partial melting and fractionation of the Palaeotethyan subducted lithosphere and lithospheric mantle; whereby, the latter must have been metasomatized by subduction-related fluids. Final steps of this model comprise the process of crustal contamination. During the Illyrian time, the earlier mentioned short-lived sedimentary basins were the places of siliciclastic limestone deposition accompanied by the sedimentation of cherts enriched in terrigenous component and interlayered with pyroclastic rocks, principally andesitic tuffs, as reported from the volcano-sedimentary record of the Cerina section at the Ivanščica Mt. (Figures 2 and 15a,b). The arc-related magmatism of the southern active European continental margin is not genetically related to the oceanic crust and ophiolites generated in the Meliata-Maliak back-arc basin.

Despite of the somewhat contrasting palinspastic restorations that are being suggested for the tectonism in the area of west Palaeotethys during mid-Triassic (e.g., Dercourt, Ricou, & Vrielynck, 1993; Harangi et al., 1996; Robertson, 2002; Stampfli & Borel, 2002, 2003, 2004; Csontos & Vörös, 2004; Bortolotti et al., 2013), there is still a high level of accordance on the contemporaneous existence of subduction and rifting-related processes in that part of Tethys. Shortly after the above described sequence of events took place along the continental rim of the northwestern segment of Palaeotethys in the Late Anisian, the uplift of mantle dome ensued, causing an adiabatic decompression and, further on, a disintegration of carbonate platform along the system of subparallel faults. This was followed by the proto back-arc rifting of the intracontinental lithosphere behind the pericontinental volcanic arc (e.g., Slovenec et al., 2010; Slovenec et al., 2011; Figures 14 and 15a). The onset of rifting created an ensialic back-arc rift basin with deep-water sediments and oceanic crust (Goričan et al., 2005; Figure 15b). The rifting produced uncontaminated primitive and evolved (OIB-type) alkali lavas devoid of crustal contamination. This calls for a significant rollback and retreat of the subducted sinking slab (Slovenec et al., 2010; Slovenec et al., 2011) pointing to the final subduction stages of the Palaeotethys, which is in line with the hypothesis of Stampfli et al. (2001) and Ziegler and Stampfli (2001). The occurrence of the Ladinian alkaline volcanism in the Dinarides (e.g., Pamić, 1982; Vishnevskaya, Djerić, & Zakariadze, 2009) and in the Bükk Mts. in Hungary (e.g., Harangi et al., 1996; Velledits, 2004, 2006) indicates a large-scale rifting of the continental lithosphere between the future Adria microplate and the continental edge of south Laurussia (represented by pieces of recent ALCAPA, Dacia, and Tisza Mega-Unit; Figures 1a and 15b). Further Ladinian events in this westernmost segment of Tethys included the terminal phase of intracontinental rifting that prograded to the initial drifting and spreading of an ensialic back-arc basin (Slovenec et al., 2011; Figure 15c). This back-arc basin made an integral part of the larger Meliata-Maliak Tethyan oceanic system developed along the southern European (Laurassia) margin during Palaeotethyan final subduction stages (Bortolotti et al., 2013; Haas, Kovács, Krystyn, & Lein, 1995; Stampfli et al., 2013; Stampfli & Borel, 2002, 2004). The oldest spreading ridge oceanic crust related to the proto-oceanic stage is represented by the presence of P-MORB-type and enriched E-MORB-type volcanic rocks (e.g., Slovenec et al., 2011; Figure 15c). The newly formed oceanic realm in this westernmost segment of Neotethys has continuously expanded during the Triassic (Ladinian to Norian) and Early Jurassic (Pliensbachian to Toarcian) leading to the formation of the new E-depleted-, T-, and N-MORB-types of oceanic crusts between the Apulian Plate (future Adria microplate) and continental margin of the southern Laurussia (future Tiszia mega-block; e.g., Slovenec et al., 2011; Bortolotti et al., 2013; Saccani et al., 2015 and references therein).

Although the model suggested herein implies the final steps of an active subduction of Palaeotethys to have taken place during the early mid-Triassic, one should nevertheless bear in mind a possibility that the Middle Triassic subsidence and volcanism were produced without a contemporaneous active subduction. Such an alternative model, proposed for the Albanide–Hellenide segment of Tethys (e.g., Saccani et al., 2015), suggests that calc-alkaline and shoshonitic rocks could have been generated by partial melting of the heterogeneous lithospheric (subcontinental) mantle, which had been metasomatized during earlier Hercynian subduction events in Late Palaeozoic.

6 | CONCLUSIONS

This research, focused on the volcano-sedimentary succession of Ivanščica Mt. in NW Croatia (the Cerina section, Figure 2), offered thorough insights to the intensive and explosive Triassic volcanic activity, concomitant with high sedimentation rates in the subsided continental environment. The section is featured by the abundance of volcanoclastic component largely consisted of andesitic and basaltic tuffs, especially in its lower portion while the intensity of volcanic activity had gradually waned toward the top of the section. An overall affluence of tuffaceous material and geochemistry of siliciclastic component are in favour of deep-water sedimentation along the rim of an oceanic space.

Radiolarian chert deposits were further on reported in the upper portion of the section, corroborating a deep-water depositional environment, and their biostratigraphic age came out with the Illyrian age of chert intercalated with pyroclastites. The airborne andesitic and basaltic tuffs are mostly vitro-crystalloclastic containing crystalloclasts of K-feldspar, plagioclase, altered pyroxene, and amphibole merged within a mass of deuteric palagonite, illite-smectite, nontronite, montmorillonite, Fe-rich mica, and calcite.

Variations in the alteration product mineralogy have been attributed to in situ eogenesis in an open hydrologic system that prevailed in the lower portion of the section and preferentially gave rise to the formation of swelling clay species. These conditions gradually evolved toward environment with restricted fluid percolation, which in turn produced parageneses richer in palagonite and micro to cryptocrystalline mica.

Mineralogy and geochemistry of tuffs were found as characteristics for magma chambers that formed in the suprasubduction zone namely, the plausible geodynamic scenario puts forth the genesis of analyzed tuffs to first include a dehydration and partial melting of down-going Palaeotethyan slab, which eventually brough in the subduction-related fluid metasomatism outlined by enrichment of LILE, Th, and LREE coupled with negative anomalies of the Nb-Ta pair, P, and Ti. Second, the contamination of parental magma must have taken place through the interaction with continental crust at the time of magma ascend through the tectonically weaken upper crust. An active, ensialic, and mature volcanic arc is hence proposed, which came into existence along the southern active continental margins of Laurussia as a result of the subduction of Palaeotethyan lithosphere during early Triassic.

ACKNOWLEDGEMENTS

The presented outcome is the result of the scientific project "Mesozoic magmatic, mantle, and pyroclastic rocks of northwestern Croatia" (Grant 181-1951126-1141 to Da. S.) carried out under the support of the Croatian Ministry of Science, Education and Sport. We wish to acknowledge the support of NSF Grant MRI 04-511 to the College of Arts and Sciences Microscopy of Texas Tech University for enabling the access to SEM-EDS equipment. Financial support for Š. Goričan was provided by the Slovenian Research Agency, Research Core Funding P1-0008. Critical comments and constructive reviews by K. Sayit and one anonymous reviewer, as well as the editorial handling by E. Bozkurt contributed significantly to the manuscript quality.

CONFLICT OF INTEREST

The authors declare no conflict of interest.

ORCID

Damir Slovenec https://orcid.org/0000-0002-6485-7930
Branimir Šegvić https://orcid.org/0000-0002-3769-7249
Giovanni Zanoni https://orcid.org/0000-0002-4303-7781

REFERENCES

Adachi, M., Yamamoto, K., & Sugisaki, R. (1986). Hydrothermal cherts and associated silicious rocks from northern Pacific: Their geological significance as indication of ocean ridge activity. *Sedimentary Geology*, *47*, 125–148.

Aljinović, D., Kolar-Jurkovšek, T., Jurkovšek, B., & Hrvatović, H. (2010). Characteristics of some Middle Triassic volcaniclastic rocks in the external Dinarides (Croatia and Bosnia and Herzegovina). In M. Horvat (Ed.), *Abstract book* (pp. 14–15). 4st Croatian Geological Congress, Šibenik, Croatian Geol. Survey.

Andreozzi, M., Dinelli, E., & Tateo, F. (1997). Geochemical and mineralogical criteria for the identification of ash layers in the stratigraphic framework of a foredeep; The early Miocene Mt. Cervarola sandstones, northern Italy. *Chemical Geology*, *137*, 23–39.

Bach, W., Peucker-Ehrenbrink, B., Hart, S. R., & Blusztajn, J. (2003). Geochemistry of hydrotermally altered oceanic crust: DSDP/ODP Hole 504B – Implications for seawater-crust excange budgets and Sr- and Pb-isotopic evolution of the mantle. *Geochemistry, Geophysics, Geosystems*, *4*, 8904. https://doi.org/10.1029/200226C000419

Bailey, J. C. (1981). Geochemical criteria for a refined tectonic discrimination of orogenic andesites. *Chemical Geology*, *32*, 139–154.

Baltuck, M. (1982). Provenance and distribution of Tethyan pelagic and hemipelagic siliceous sediments, Pindos mountains, Greece. *Sedimentary Geology*, *31*, 63–88.

Bébien, J., Blanchet, R., Cadet, J. P., Charvet, J., Chorowitz, J., Lapierre, H., & Rampnoux, J. P. (1978). Le volcanisme triasique des Dinarides en Yougoslavie: Sa place dans l'évolution géotectonique périméditerrenéenne. *Tectonophysics*, *47*, 159–176.

Bishop, J. L., Schiffman, P., & Southard, R. (2002). Geochemical and mineralogical analyses of palagonitic tuffs and altered rinds of pillow basalts in Iceland and applications to Mars. *Geological Society, Special Publication*, *202*, 371–392.

Bonadiman, C., Coltorti, M., & Siena, F. (1994). Petrogenesis and T-fO2 estimates of Mt. Monzoni complex (Central Dolomites, Southern Alps): A Triassic shoshonotic intrusion in a transcurrent geodynamic setting. *European Journal of Mineralogy*, *6*, 943–966.

Borojević-Šoštarić, S., Neubauer, F., Handler, F., & Palinkaš, L. A. (2012). Tectonothermal history of the basement rocks within the NW Dinarides: New $^{40}Ar/^{39}Ar$ ages and synthesis. *Geologica Carpathica*, *63*, 441–452.

Bortolotti, V., Chiari, M., Marroni, M., Pandolfi, L., Principi, G., & Saccani, E. (2013). The geodynamic evolution of the ophiolites from Albania and Greece, Dinaric-Hellenic Belt: One, two, or more oceanic basins? *International Journal of Earth Sciences*, *102*, 783–811. https://doi.org/10.1007/s00531-012-0835-7

Brack, P., Rieber, H., Nicora, A., & Mundil, R. (2005). The Global boundary Stratotype Section and Point (GSSP) of the Ladinian Stage (Middle Triassic) at Bagolino (Southern Alps, Northern Italy) and its implications for the Triassic time scale. *Episodes*, *28*, 233–244.

Cas, R. A. F., & Wright, J. V. (1987). *Volcanic successions modern and ancient: A geological approach to processes, products and successions* (p. 528). London: Chapman and Hall.

Casetta, F., Coltorti, M., & Marrocchino, E. (2018). Petrological evolution of the Middle Triassic Predazzo intrusive complex, Italian Alps. *International Geology Review*, *60*, 977–997.

Castellarin, A., Lucchini, F., Rossi, P. L., Selli, L., & Simboli, G. (1988). The Middle Triassic magmatic-tectonic arc developed in the Southern Alps. *Tectonophysics*, *146*, 79–89.

Castellarin, A., Lucchini, F., Rossi, P. L., Simboli, G., Bosellini, A., & Sommavilla, E. (1980). Middle Triassic magmatism in Southern Alps II: A geodynamic model. *Rivista Italiana di Paleontologia e Stratigrafia*, *85*, 3–4.

Chamley, P. D. H. (1989). Paleoenvironmental reconstruction. In *Clay Sedimentology* (pp. 487–526). Berlin, Heidelberg: Springer-Verlag.

Chapin, C. E., & Lindley, J. I. (1985). Potassium metasomatism of volcanic and sedimentary rocks in rift basins, calderas and detachment terranes. In *Presented at the Heat and Detachment in Crustal Extension on*

Continents and Planets (pp. 25–31). Houston, USA: Lunar and Planetary Institute.

Chiari, M., Bortolotti, V., Marcucci, M., Photiades, A., Principi, G., & Saccani, E. (2012). Radiolarian biostratigraphy and geochemistry of the Koziakas massif ophiolites (Greece). *Bulletin de la Société géolgique de France*, *183*, 287–306.

Chiari, M., Marcucci, M., Cortese, G., Ondrejičkova, A., & Kodra, A. (1996). Triassic rediolarian assemblages in the Rubik area and Cukali Zone, Albania. *Ofioliti*, *21*, 77–84.

Christidis, G. E. (1998). Comparative study of the mobility of major and trace elements during alteration of an andesite and a rhyolite to bentonite, in the Islands of Milos and Kimolos, Aegean, Greece. *Clays and Clay Minerals*, *46*, 379–399.

Christidis, G. E., & Huff, W. D. (2009). Geological aspects and genesis of bentonites. *Elements*, *5*, 93–98.

Coogan, L. A. (2009). Altered oceanic crust as an inorganic record of paleoseawater Sr concentration. *Geochemistry*, *Geophysics*, *Geosystems*, *10*, Q04001. https://doi.org/10.1029/2008GC002341

Crisci, C. M., Ferrara, G., Mazzuoli, R., & Rossi, P. M. (1984). Geochemical and geochronological data on Triassic volcanism in the Southern Alps of Lombardy (Italy): genetic implications. *Geologische Rundschau*, *73*, 279–292.

Csontos, L., & Vörös, A. (2004). Mesozoic plate tectonic reconstruction of the Charpatian region. *Palaeogeography*, *Palaeoclimatology*, *Palaeoecology*, *210*, 1–56.

De Bono, A., Martini, R., Zaninetti, L., Hirsch, F., Stampfli, G. M., & Vavassis, I. (2001). Permo-Triassic stratigraphy of the Palagonian zone in central Evia island (Greece). *Eclgae geologicae Helvetiae*, *94*, 289–311.

Del Piaz, G. V., & Martin, S. (1998). Evoluzione litosferica e magmatismo nel dominio austro-sudalpino dall'orogenesivarisica al rifting permo-mesozoico. Riunione estiva S.G.I. *Memorie della Societa Geologia Italiana*, *53*, 43–62.

Dercourt, J., Ricou, L. E., & Vrielynck, B. (1993). Atlas of Tethys palaeoenvironmental maps: Paris, *Commision de le Carte géologique du monde*, 307 pp + maps.

Dosztály, L., & Jozsa, S. (1992). Geochronologichal evaluation of mesozoic formations of Darnó Hill at Recsk on the basis of radiolarians and K-Ar age data. *Acta Geologica Hungarica*, *35*, 371–393.

Dumitrica, P. (1982). Triassic Oertlisponginae (Radiolaria) from Eastern Carpathians and Southern Alps. *Dari de seama ale sedintelor*, *Institutul de Geologie si Geofizica*, *Bucuresti*, *67*, 57–74.

Dumitrica, P. (1999). The Oertlispongidae (Radiolaria) from the Middle Triassic of Masirah Island (Oman). *Revue de Micropaleontologie*, *42*, 33–42.

Elburg, M. A., Bergin, M. V., Hoogewerff, J., Folden, J., Vroon, P., Zulkarnain, I., & Nasution, A. (2002). Geochemical trends accros an arc-continent collision zone: Magma sources and slab-wedge transfer processes below the Pantar Strait volcanoes, Indonesia. *Geochimica et Cosmochimica Acta*, *66*, 2771–2789.

Fisher, R. V., & Schmincke, H. U. (1984). *Pyroclastic rocks*. Berlin: Springer-Verlag.

Frisch, W., Meschede, M., & Blakey, R. (2011). *Plate tectonics: Continental drift and Mountain Building*. Berlin: Springer-Verlag.

Gawlick, H. J., Goričan, Š., Missoni, S., Dumitrica, P., Lein, R., Frisch, W., & Hoxha, L. (2016). Middle and Upper Triassic radiolarite components from the Kcira-Dushi-Komani ophiolitic mélange and their provenance (Mirdita Zone, Albania). *Revue de Micropaleontologie*, *59*, 359–380.

Girty, G. H., Ridge, D. L., Knaack, C., Johnson, D., & Al-Riyami, R. K. (1996). Provenance and depositional setting of Paleozoic chert and argillite, Sierra Nevada, California. *Journal of Sedimentary Research*, *66*(1), 107–118.

Golub, LJ., & Brajdić, V. (1970). Eruptive and pyroclastic rocks from Vudelja and from the Bistrica brook on the northern slopes of Mt. Ivanščica (Hrvatsko Zagorje – Yugoslavia). *Zbornik radova Rudarsko-geološko-naftnog fakulteta* (30. god. rada, 1939-1969), 123-127 (in Croatian, with English abstract).

Goričan, Š., Halamić, J., Grgasović, T., & Kolar-Jurkovšek, T. (2005). Stratigraphic evolution of Triassic arc-backarc system in northwestern Croatia. *Bulletin de la Société géolgique de France*, *176*, 3–22.

Gorton, M. P., & Shandl, E. S. (2000). From continents to island arcs: A geochemical indeks of tectonic setting for arc-related and within-plate felsic to intermediate volcanic rocks. *The Canadian Mineralogist*, *38*, 1065–1073.

Grimes, C. B., Wooden, J. L., Cheadle, M. J., & John, B. E. (2015). "Fingerprinting" tectono-magmatic provenance using trace elements in igneous zircon. *Contributions to Mineralogy and Petrology*, *170*(46).

Haas, J., Kovács, S., Krystyn, L., & Lein, R. (1995). Significance of Late Permian – Triassic facies zones in terrane reconstructions in the Alpine – North Pannonian domain. *Tectonophysics*, *242*, 19–40.

Haas, J., Mioč, P., Pamić, J., Tomljenović, B., Árkai, P., Bérczi-Makk, A., … R-Felgenhauer, E. (2000). Complex structural pattern of the Alpine-Dinaridic Pannonian triple junction. *International Journal of Earth Sciences*, *89*, 377–389.

Haas, J., Pelikán, P., Gorog, Á., Ozsvárt, P., Jósza, S., & Kovér, S. (2010). Subduction related Jurassic gravity deposits in Bükk-Darnó area. Northeast. *Scientific Annals of the School of Geology*, *Aristotale University of Thessaloniki*, *100*, 149–156.

Halamić, J. (1998). The lithostratigraphic characterisation of Jurassic and Cretaceous sediments with ophiolite of Mts. Medvednica, Kalnik and Ivanščica. PhD Thesis, Zagreb University, 1-184 (in Croatian, with English abstract).

Halamić, J., & Goričan, Š. (1995). Triassic radiolarites from Mts. Kalnik and Medvednica (Northwestern Croatia). *Geologia Croatica*, *48*, 129–146.

Halamić, J., Marchig, V., & Goričan, Š. (2001). Geochemistry of Triassic radiolarian cherts in north-western Croatia. *Geologica Carpathica*, *52*, 327–342.

Halamić, J., Slovenec, D., & Kolar-Jurkovšek, T. (1998). Triassic pelagic limestones in pillow lavas in the Orešje quarry near Gornja Bistra, Medvednica Mt. (Northwest Croatia). *Geologia Croatica*, *51*, 33–45.

Harangi, S., Szabó, C., Józsa, S., Szoldán, Z., Árva-Sós, E., Balla, M., & Kubovics, I. (1996). Mesozoic igneous suites in Hungary: Implications for genesis and tectonic setting in the northwestern part of Tethys. *International Geology Review*, *38*, 336–360.

Hawkesworth, C. J., Gallagher, K., Hergt, J. M., & McDermott, F. (1993). Trace element fractionation processes in the generation of island arc basalts. In K. G. Cox, D. P. McKenzie, & R. S. White (Eds.), *Melting and melt movement in the Earth* (pp. 179–191). Oxford and London A342: Philosophical Transactions of Royal Society London, Oxford University Press.

Hawkesworth, C. J., Turner, S. P., McDermott, F., Peate, D. W., & Van Calsteren, P. (1997). U-Th isotopes in arc magmas: Implications for element transfer from the subducted crust. *Science*, *276*, 551–555.

Huppert, H. E., & Stephen, R. J. (1985). Cooling and contamination of mafic and ultramafic magmas during ascent through continental crust. *Earth and Science Planetary Letters*, *74*, 371–386.

Ivan, P. (2002). Relics of the Meliata ocean crust: Geodynamic implications of mineralogical. *petrological and geochemical proxies*. *Geologica Carpathica*, *53*, 245–256.

Jordan, P., & Rippey, B. (2003). Lake sedimentary evidence of phosphorus, iron and manganese mobilisation from intensively fertilised soils. *Water Research*, *37*, 1426–1432.

Kiss, G., Molnár, F., Palinkaš, L., Kováacs, S., & Hrvatović, H. (2012). Correlation of Triassic advanced rifting-related Neotethyan submarine basaltic volcanism of the Darnó Unit (NE-Hungary) with some Dinaridic and Hellenidic occurrences on the basis of volcanological, fluid–rock interaction, and geochemical characteristics. *International Journal of Earth Sciences*, *101*, 1503–1521.

Knežević, V., Jovanović, V., Memović, E., & Resimović, K. (1998). Triassic magmatic rocks of Yugoslav Dinarides – in Serbia. *XIII kongres geologa Jugoslavije, Herceg Novi, Zbornik radova 3*, 61-66 (in Serbian, with English abstract).

Kovács, S. (1989). Major events of the tectono-sedimentary evolution of the north Hungarian Paleo-Mesozoic: History of the NW termination of the Late Paleozoic-Early Mesozoic Tethys. In A. M. C. Segnör (Ed.), *Tectonic evolution of the Tethyan region* (Vol. 259). *Series C: Mathematical and Phisical Sciences*. (pp. 93–108). London: Klaver Academic Publisher.

Kovács, S. (1992). Tethys "western ends" during the late Paleozoic and Triassic and their possible genetic relationships. *Acta Geologica Hungarica*, *35*, 329–369.

Kozur, H. (1991). The evolution of the Meliata-Hallstatt ocean and its significance for the early evolution of the Eastern Alps and western Carpathians. *Paleogeography, Palaeoclimatology, Palaeoecology*, *87*, 109–135.

Kozur, H., & Mostler, H. (1994). Anisian to Middle Carnian radiolarian zonation and description of some stratigraphically important radiolarians. *Geologisch-Paläontologische Mitteilungen Innsbruck, Sonderband*, *3*, 39–255.

Kozur, H. W. (2003). Integrated ammonoid, conodont and radiolarian zonation of the Triassic. *Hallesches Jahrbuch für Geowissenschaften*, *25*, 49–79.

Kozur, H. W., Krainer, K., & Mostler, H. (1996). Radiolarians and facies of the Middle Triassic Loibl Formation, South Alpine Karawanken Mountains (Carinthia, Austria). *Geologisch-Paläontologische Mitteilungen Innsbruck, Sonderband*, *4*, 195–269.

Kunimaru, T., Shimizu, H., Takahashi, K., & Yabuki, S. (1998). Differences in geochemical features between Permian and Triassic cherts from the Southern Chichibu terrane, southwest Japan: REE abundances, major element compositions and Sr isotopic ratios. *Sedimentary Geology*, *119*, 195–217.

Lawrence, J. R., Drever, J. I., Anderson, T. F., & Brueckner, H. K. (1979). Importance of alteration of volcanic material in the sediments of Deep Sea Drilling Site 323: Chemistry, O^{18}/O^{16} and Sr^{87}/Sr^{86}. *Geochimica et Cosmochimica Acta*, *43*, 573–588.

Leyrit, H., & Montenat, C. (2000). *Volcaniclastic rocks, from magmas to sediments*. Amsterdam: Gordon and Breach Science Publischers, CRC Press.

Marci, V., Šćavničar, S., & Sijarić, G. (1982). Petrogenesis of the volcanic rocks of Ivanščica Mt. (River Željeznica). *X kongres geologa Jugoslavije, Budva, Zbornik radova 1*, 329-335 (in Croatian, with English abstract).

Marci, V., Ščavnićar, S., & Sijarić, G. (1984). The new data about volcanic rocks of Ivanščica mountain. *Geoloski Vjesnik*, *37*, 97–104. (in Croatian, with English abstract)

McCann, T. (2008). *The geology of Central Europe* (Vol. 2). *Mesozoic and Cenosoic*. (p. 1491). London: The Geological Society London.

Moore, D. M., & Reynolds, R. C. (1997). *X-ray diffraction and the identification and analysis of clay minerals* (2nd ed.). Oxford: University Press.

Müller, D., Rock, N. M. S., & Groves, D. I. (1992). Geochemical discrimination between shoshonitic and potassic volcanic rocks in different tectonic settings: A pilot study. *Mineralogy and Petrology*, *46*, 259–289.

Mundil, R., Pálfy, J., Renne, P. R., & Brack, P. (2010). The Triassic timescale: New constraints and a review of geochronological data. In S. G. Lucas (Ed.), *The Triassic Timescale* (Vol. 334). *Special Publications*. (pp. 41–60). London: Geological Society London.

Murray, R. W. (1994). Chemical criteria to identify the depositional environment of chert: General principles and applications. *Sedimentary Geology*, *90*, 213–232.

Murray, R. W., Buchholtz, T. B., Marilyn, R., Gerlach, D. C., Price, R. G. III, & Jones, D. L. (1991). Rare earth, major, and trace elements in chert from the Franciscan Complex and Monterey Group, California: Assessing REE sources to fine-grained marine sediments. *Geochimica et Cosmochimica Acta*, *55*, 1875–1895.

Obenholzner, J. H. (1991). Triassic volcanogenic sediments from the Southern Alps (Italy, Austria, Yugoslavia) – A contribution to the "Pietra verde" problem. *Sedimentary Geology*, *74*, 147–171.

Ozsvárt, P., & Kovács, S. (2012). Revised Middle and Late Triassic radiolarian ages for ophiolite melanges: Implications for the geodynamic evolution of the northern part of the early Mesozoic Neotethyan subbasins. *Bulletin de la Société géolgique de France*, *183*, 273–286.

Pamić, J. (1982). Correlation between Mesozoic spilite–keratophyre associations of the continental and oceanic crust origin as exemplified by the Dinarides. *Earth Evolution Sciences*, *2*, 36–40.

Pamić, J. (1984). Triassic magmatism of the Dinarides in Yugoslavia. *Tectonophysics*, *109*, 273–307.

Pamić, J. (1997). *Volcanic rocks from the Sava-Drava interfluve and Baranja in the south Pannonian basin (Croatia)*. Zagreb: Nafta.

Pamić, J., & Balen, D. (2005). Interaction between permo-Triassic rifting, magmatism and initiation of the Adriatic-Dinaridic carbonate platform (ADCP). *Acta Geologica Hungarica*, *48*, 181–204.

Pamić, J., & Tomljenović, B. (1998). Basic geological data on the Croatian part of the Mid-Transdanubian Zone as exemplified by Mt. Medvednica located along the Zagreb-Zemplen Fault Zone. *Acta Geologica Hungarica*, *41*, 389–400.

Pearce, J. A. (1975). Basalt geochemistry used to investigate past tectonic environments on Cyprus. *Tectonophysics*, *25*, 41–67.

Pearce, J. A. (1983). Role of the sub-continental lithosphere in magma genesis at active continental margins. In C. J. Hawkesworth, & M. J. Norry (Eds.), *Continental basalts and mantle xenoliths* (pp. 230–249). Nantwich UK: Shiva.

Pe-Piper, G. (1998). The nature of Triassic extension-related magmatism in Greece: Evidence from Nd and Pb isotope geochemistry. *Geological Magazine*, *135*, 331–348.

Philip, J., Masse, J.-P., & Camoin, G. (1995). Tethyan carbonate platforms. In A. E. M. Nairn, L. E. Ricov, B. Vrielynck, & J. Dércourt (Eds.), *The ocean basins and margins* (Vol. 8) (pp. 239–265). New York: Plenum Press.

Pomonis, P., Tsikouras, V., & Hatzipanagiotou, K. (2004). Comparative geochemical study of the Triassic trachyandesites of Glykomilia and alkali basalts from the Koziakas ophiolite mélange (W. Thessaly): Implications for their origin. *Bulletin of the Geological Society of Greece*, *36*, 587–596.

Rajaraman, H. S., Nagendra Babu, G., Chavan, S. J., Achar, K. K., & Ramesh Babu, P. V. (2013). Signature of potassium enrichment in granite of the Chitrial area, Nalgonda district, Andhra Pradesh: Inferences using its U, Th, K_2O, Na_2O, Rb, Ba and Sr contents. *Journal of the Geological Society of India*, *82*, 53–58.

Rangin, C., Steinberg, M., & Bonnot-Courtois, C. (1981). Geochemistry of the Mesozoic bedded chert of Central Baja California (Vizcaino-Cedros-San Benito): implications for paleogeographic reconstruction of an old oceanic basin. *Earth and Planetary Science Letters*, *54*, 313–322.

Robertson, A. H. F. (2002). Overview of the genesis and emplacement of Mesozoic ophiolites in the eastern Mediterranean Tethyan region. *Lithos*, *65*, 1–67.

Robertson, A. H. F. (2007). Overview of tectonic settings related to the rifting and opening of mesozoic ocean basins in the eastern Tethys: Oman, Himalayas and Eastern Mediterranean regions. *Geological Society of London, Special Publication*, *282*, 325–388.

Rudnick, R. L., & Fountain, D. M. (1995). Nature and composition of the continental crust: A lower crustal perspective. *Reviews of Geophysics*, *33*, 267–309.

Ruitz-Ortiz, P. A., Bustillo, M. A., & Molina, J. M. (1989). Radiolarite sequences of the Subbetic, Betic Cordillera, Southern Spain. In J. R. Hein, & J. Obradović (Eds.), *Siliceous deposits of the Tethys and Pacific regions* (pp. 107–127). Berlin: Springer-Verlag.

Saccani, E., Dilek, Y., Marroni, M., & Pandolfi, L. (2015). Continental margin ophiolites of Neotethys: Remnants of Ancient Ocean–Continent Transition Zone (OCTZ) lithosphere and their geochemistry, mantle sources and melt evolution patterns. *Episodes*, *38*, 230–249.

Ščavničar, B., Ščavničar, S., & Šušnjara, A. (1984). The volcanic-sedimentary Middle Triassic in the Suvaja brook area (Mt. Svilaja, Outer Dinarides). *Acta Geologica*, *14*, 35–82.

Schmid, S. M., Bernoulli, D., Fügenschuh, B., Matenco, L., Scheffer, S., Schuster, R., … Ustaszewski, K. (2008). The Alpine-Carpathian-Dinaridic orogenic system: Correlation and evolution of tectonic units. *Swiss Journal of Geosciences*, *101*, 139–183.

Schmid, S. M., Fügenschuh, B., Kissling, E., & Schuster, R. (2004). Tectonic map overall architecture of the Alpine orogen. *Eclogea geologicea Helvetiae*, *97*, 93–117.

Schminke, H. U. (2004). *Volcanism*. Berlin: Springer-Verlag.

Šegvić, B., Mileusnić, M., Aljinović, D., Vranjković, A., Mandic, O., Pavelić, D., … Ferreiro Mählmann, R. (2014). Magmatic provenance and diagenesis of Miocene tuffs from the Dinaride Lake System (the Sinj Basin, Croatia). *European Journal of Mineralogy*, *26*, 83–101. https://doi.org/10.1127/0935-1221/2013/0025-2350

Shervais, J. W. (1982). Ti-V plots and petrogenesis of modern and ophiolitic lavas. *Earth and Planetary Science Letters*, *59*, 101–118.

Shimizu, H., Kunimaru, T., Yoneda, S., & Adachi, M. (2001). Sources and depositional environments of some Permian and Triassic cherts: Significance of Rb-Sr and Sm-Nd isotopic and REE abundance data. *Jourrnal of Geology*, *109*, 105–125.

Šimunić, A. (1992). Geological relations of the central part of the Croatian Zagorje. PhD Thesis, Zagreb University, 1-189 (in Croatian, with English abstract).

Šimunić, An., Pikija, M., & Hećimović, I. (1982). Basic geological map 1:100.000. Sheet Varaždin, Institut za geološka istraživanja Zagreb - Savezni geološki zavod Beograd.

Šimunić, A., & Šimunić, A. (1979). Petrographic composition and genesis of Triassic deposits of Ivanščica, Kalnik and Ravna gora Mt. *Geoloski Vjesnik*, *32*, 243–253. (in Croatian, with English abstract)

Singer, A. (1974). Mineralogy of palagonitic material from the Golan Heights, Israel. *Clays and Clay Minerals*, *22*, 231–240. https://doi.org/10.1346/CCMN.1974.0220305

Slovenec, D., Lugović, B., Meyer, P., & Garapić-Šiftar, G. (2011). A tectonomagmatic correlation of basaltic rocks from ophiolite mélanges at the north-eastern tip of the Sava-Vardar suture Zone, Northern Croatia, constrained by geochemistry and petrology. *Ofioliti*, *36*, 77–100.

Slovenec, D., Lugović, B., & Vlahović, I. (2010). Geochemistry, petrology and tectonomagmatic significance of basaltic rocks from the ophiolite mélange at the NW External-Internal Dinarides junction (Croatia). *Geologica Carpathica*, *61*, 273–294.

Smirčić, D. (2017). *Genesis of Middle Triassic volcaniclastic deposits in the external Dinarides*. PhD Thesis, Zagreb University, 1-217 (in Croatian, with English abstract).

Smirčić, D., Aljinović, D., Hrvatović, H., Barudžija, U., Kolar-Jurkovšek, T., & Jurkovšek, B. (2017). In L. Sahakyan, A. Baud, A. Grigoryan, E. Friesenbichler, & S. Richoz (Eds.), *The geotectonic evolution of the Dinaridic part of Western Tethys from Early Permian to Late Triassic. IGCP 630: Permian-Triassic climatic and environmental extremes and biotic response, IGCP630 5th International Conference, Conference Programme* (pp. 32–32). Yerevan: National Academy of Sciences of Republic of Armenia, Institute of Geological Sciences.

Sottli, G., Palladino, D. M., Cuffaro, M., & Doglioni, C. (2015). Earth's rotation variability triggers explosive eruptions in subduction zones. *Earth, Planets and Space*, *67*, 208. https://doi.org/10.1186/s40623-015-0375-z

Środoń, J. (2006). Identification and quantitative analysis of clay minerals. In F. Bergaya, B. Theng, & G. Lagaly (Eds.), *Handbook of Clay Science* (Vol. 1) (pp. 765–787). Amsterdam: Elsevier Ltd.

Stampfli, C., Hochard, C., Vérard, C., Wilhem, J., & von Raumer, J. F. (2013). The formation of Pangea. *Tectonophysics*, *593*, 1–19.

Stampfli, G.M., & Borel, G. (2003). AAPG International Conference, Barcelona, Spain.

Stampfli, G. M., & Borel, G. D. (2002). A plate tectonic model for the Paleozoic and Mesozoic constrained by dynamic plate boundaries and restored synthetic ocean isochrons. *Earth and Planetary Science Letters*, *196*, 17–33.

Stampfli, G. M., & Borel, G. D. (2004). The TRANSMED transects in space and time: Constraints on the paleotectonic evolution of the Mediterranean domain. In W. Cavazza, F. Roure, W. Spakman, G. M. Stampfli, & P. A. Ziegler (Eds.), *The TRANSMED Atlas: the Mediterranean Region from crust to mantle* (pp. 53–80). Berlin: Springer-Verlag.

Stampfli, G. M., Mosar, J., Pillevuit, A., & Vannay, J. C. (2001). Permo-Mesozoic evolution of the western Tethys realm: The Neo-Tethys East Mediterranean Basin connection. In P. A. Ziegler, W. Cavazza, A. H. F. Robertson, & S. Crasquin-Soleau (Eds.), *Peri-Tethys Memoir 6: Peri-Tethyan rift/wrench basins and passive margins* (Vol. 186) (pp. 51–108). Paris: Mém Mus natn Hist nat.

Staudigel, H., Plank, T., White, B., & Schmincke, H. U. (1996). Geochemical fluxes during sea floor alteration of the basaltic upper oceanic crust: DSDP Sites 417 and 418. In E. Bebout, D. W. Scholl, & S. H. Kirby (Eds.), *Subduction: Top to Bottom* (Vol. 96) (pp. 19–38). Washington, DC: American Geophysical Union Geophysical Monograph.

Storck, J. C., Brack, P., Jörn-Frederik Wotzlaw, J. F., & Ulmer, P. (2018). Timing and evolution of Middle Triassic magmatism in the Southern Alps (Northern Italy). *Journal of the Geological Society*, *176*, 253–268. https://doi.org/10.1144/jgs2018-123

Sugisaki, R., Yamamoto, K., & Adachi, M. (1982). Triassic bedded cherts in central Japan are not pelagic. *Nature*, *298*, 644–647.

Sugitani, K., Yamamoto, K., Wada, H., Binu-Lal, S. S., & Yoneshige, M. (2002). Geochemistry of Archean carbonaceous cherts deposited at immature island-arc setting in the Pilbara Block, Western Australia. *Sedimentary Geology*, *151*, 45–66.

Sun, S. S., & McDonough, W. F. (1989). Chemical and isotopic systematics of oceanic basalts: Implications for mantle composition and processes. In A. D. Saunders, & M. J. Norry (Eds.), *Magmatism in Ocean Basins. Geological Society* (Vol. 42) (pp. 313–345). London: Special Publications.

Sun, S. S., & Nesbitt, R. W. (1978). Geochemical regularities and genetic significance of ophiolitic basalts. *Geology*, *6*, 689–693.

Swinden, H. S., Jenner, G. A., Fryer, B. J., Hertogen, J., & Roddick, J. C. (1990). Petrogenesis and paleotectonic history of the Wild Bight

Group, an Ordovician rifted island arc in central Newfoundland. *Contributions to Mineralogy and Petrology*, *105*, 219–241.

Taylor, S. R., & McLennan, S. M. (1985). *The continental crust: Its composition and evolution*. Carlton: Blackwell Scientific Publication.

Tekin, U. K., Göncüoglu, M. C., & Turhan, N. (2002). First evidence of Late Carnian radiolarians from the Izmir-Ankara suture complex, central Sakarya, Turkey: Implications for the opening age of the Izmir-Ankara branch of Neo-Tethys. *Geobios*, *35*, 127–135.

Trubelja, F., Burgath, K. P., & Marchig, V. (2004). Triassic magmatism in the area of the Central Dinarides (Bosnia and Herzegovina): Geochemical resolving of tectonic setting. *Geologia Croatica*, *57*, 159–170.

Velde, B. D. (1995). *Origin and mineralogy of clays: Clays and the environment*. Berlin, Heidelberg, New York: Springer-Verlag.

Velledits, F. (2004). Anisian terrestrial sediments in the Bükk Mountains (NE Hungary) and their role in the Triassic rifting of the Vadar-Meliata branch of Neo-Tethys ocean. *Rivista Italiana di Paleontologia e Stratigrafia*, *110*, 659–679.

Velledits, F. (2006). Evolution of Bükk Mountains (NE Hungary) during the Middle-Late Triassic asymmetric rifting of the Vadar-Meliata branch of the Neotethys Ocean. *International Journal of Earth Sciences*, *95*, 395–412.

Vine, J. D. (1969). Element distribution in some Paleozoic black shales and associated rocks. *Contribution to Geochemistry*, *Geological Survey Bulletin*, *1214-G*, 329–581.

Vishnevskaya, V. S., Djerić, N., & Zakariadze, G. S. (2009). New data on Mesozoic Radiolaria of Serbia and Bosnia, and implications for the age and evolution of oceanic volcanic rocks in the central and northern Balkans. *Lithos*, *108*, 72–105.

Vlahović, I., Tišljar, J., Velić, I., & Matičec, D. (2005). Evolution of the Adriatic carbonate platform: Paleogeography, main events and depositional dynamics. *Palaeogeography*, *Palaeoclimatology*, *Palaeoecology*, *220*, 333–360.

Wilson, M. (1989). *Igneous petrogenesis*. London: Unwin Hyman Ltd.

Winchester, J. A., & Floyd, P. A. (1977). Geochemical discrimination of different magma series and their differentiation products using immobile elements. *Chemical Geology*, *20*, 325–343.

Wood, D. A. (1980). The application of a Th-Hf-Ta diagram to problems of tectonomagmatic classification and establishing the nature of crustal contamination of basaltic lavas of the British tertiary volcanic province. *Earth and Planetary Science Letters*, *50*, 11–30.

Zhao, L., Zhu, Q., Jia, S., Zou, J., Nechaev, V. P., & Dai, S. (2017). Origin of minerals and critical metals in an argillized tuff from the Huayingshan Coalfield, Southwestern China. *Minerals*, *7*, 92. https://doi.org/10.3390/min7060092

Ziegler, P. A., & Stampfli, G. M. (2001). Late Paleozoic–early Mesozoic plate boundary reorganization: Collapse of the Variscan orogen and opening of Neotethys. *Natura Bresciana Ann Mus Civ Sc Nat*, *Monografia*, *25*, 17–34.

How to cite this article: Slovenec D, Šegvić B, Halamić J, Goričan Š, Zanoni G. An ensialic volcanic arc along the northwestern edge of Palaeotethys—Insights from the Mid-Triassic volcano-sedimentary succession of Ivanščica Mt. (northwestern Croatia). *Geological Journal*. 2020;55:4324–4351. https://doi.org/10.1002/gj.3664